Published August 13, 2012

Fission yeast Ags1 confers the essential septum strength needed for safe gradual cell abscission

Juan Carlos G. Cortés,[1] Mamiko Sato,[3] Javier Muñoz,[1] M. Belén Moreno,[1] Jose Angel Clemente-Ramos,[1] Mariona Ramos,[1] Hitoshi Okada,[2] Masako Osumi,[2,3] Angel Durán,[1] and Juan Carlos Ribas[1]

[1]Instituto de Biología Funcional y Genómica, Consejo Superior de Investigaciones Científicas (CSIC)/Universidad de Salamanca, 37007 Salamanca, Spain
[2]Integrated Imaging Research Support (IIRS), Villa Royal Hirakawa 103, 1-7-5 Hirakawa-cho, Chiyoda-ku Tokyo, Japan
[3]Laboratory of Electron Microscopy/Bio-imaging Center, Japan Women's University, 2-8-1 Mejirodai, Bunkyo-ku Tokyo, Japan

Fungal cytokinesis requires the assembly of a dividing septum wall. In yeast, the septum has to be selectively digested during the critical cell separation process. Fission yeast cell wall α(1-3)glucan is essential, but nothing is known about its localization and function in the cell wall or about cooperation between the α- and β(1-3)glucan synthases Ags1 and Bgs for cell wall and septum assembly. Here, we generate a physiological Ags1-GFP variant and demonstrate a tight colocalization with Bgs1, suggesting a cooperation in the important early steps of septum construction. Moreover, we define the essential functions of α(1-3)glucan in septation and cell separation. We show that α(1-3)glucan is essential for both secondary septum formation and the primary septum structural strength needed to support the physical forces of the cell turgor pressure during cell separation. Consequently, the absence of Ags1 and therefore α(1-3)glucan generates a special and unique side-explosive cell separation due to an instantaneous primary septum tearing caused by the turgor pressure.

Introduction

Fungal cytokinesis requires concomitant contractile actomyosin ring (CAR) closure and the synthesis of a special cell wall structure termed septum (Pollard and Wu, 2010). *Schizosaccharomyces pombe* medial fission displays several stages: CAR positioning and assembly, activation of CAR contraction and septum formation by the septation initiation network (SIN), septum synthesis, and cell separation (Sipiczki, 2007; Krapp and Simanis, 2008). The septum is a three-layered structure composed of a middle disk named primary septum, flanked at both sides by the secondary septum (Johnson et al., 1973). The last step of cytokinesis is cell separation that requires degradation of the primary septum and the adjacent cell wall (septum edging) by glucanases. Therefore, correct assembly and structural integrity of the septum are vital for cell survival.

The fission yeast cell wall consists of an outer layer rich in galactomannoproteins and an inner layer comprised of β(1-3), β(1-6), and α(1-3)glucans (Pérez and Ribas, 2004; Grün et al., 2005). Immunoelectron microscopy (IEM) studies delimited the branched β(1-6)glucan in the cell wall and secondary septum, the branched β(1-3)glucan in the cell wall and both primary and secondary septum, and a linear β(1-3)glucan (L-BG) mainly present in the primary septum and a small amount in the cell wall (Humbel et al., 2001; Cortés et al., 2007). L-BG is necessary but not sufficient for primary septum formation and is the polysaccharide that specifically interacts with the fluorochrome Calcofluor white (CW) in *S. pombe* (Cortés et al., 2007). In addition to β-glucans, other polysaccharides, like the α(1-3)glucan, may be present in the primary septum as well. α(1-3) and branched β(1-3)glucans are essential for cell shape maintenance. However, their importance for cell wall and septum structure and function is still unknown (Ribas et al., 1991; Hochstenbach et al., 1998; Katayama et al., 1999).

S. pombe contains three essential β(1-3)glucan synthases (βGSs) that localize in CAR, septum, growing poles, and sites of wall synthesis during sexual differentiation. Bgs1 appears earlier in the division site and is responsible for the L-BG and primary septum synthesis. Bgs4 is essential for cell integrity and is the only subunit shown to form part of the βGS enzyme. Bgs3 function remains unknown (Cortés et al., 2002, 2005, 2007; Liu et al., 2002; Martín et al., 2003; Martins et al., 2011).

Correspondence to Juan Carlos G. Cortés: cortes@usal.es

Abbreviations used in this paper: CAR, contractile actomyosin ring; CW, Calcofluor white; GS, glucan synthase; ICW, internal cell wall; L-BG, linear β(1-3)glucan; SIN, septation initiation network; WT, wild type.

Supplemental Material can be found at:
http://jcb.rupress.org/content/suppl/2012/08/09/jcb.201202015.DC1.html

The Rockefeller University Press $30.00
J. Cell Biol. Vol. 198 No. 4 637–656
www.jcb.org/cgi/doi/10.1083/jcb.201202015

Published August 13, 2012

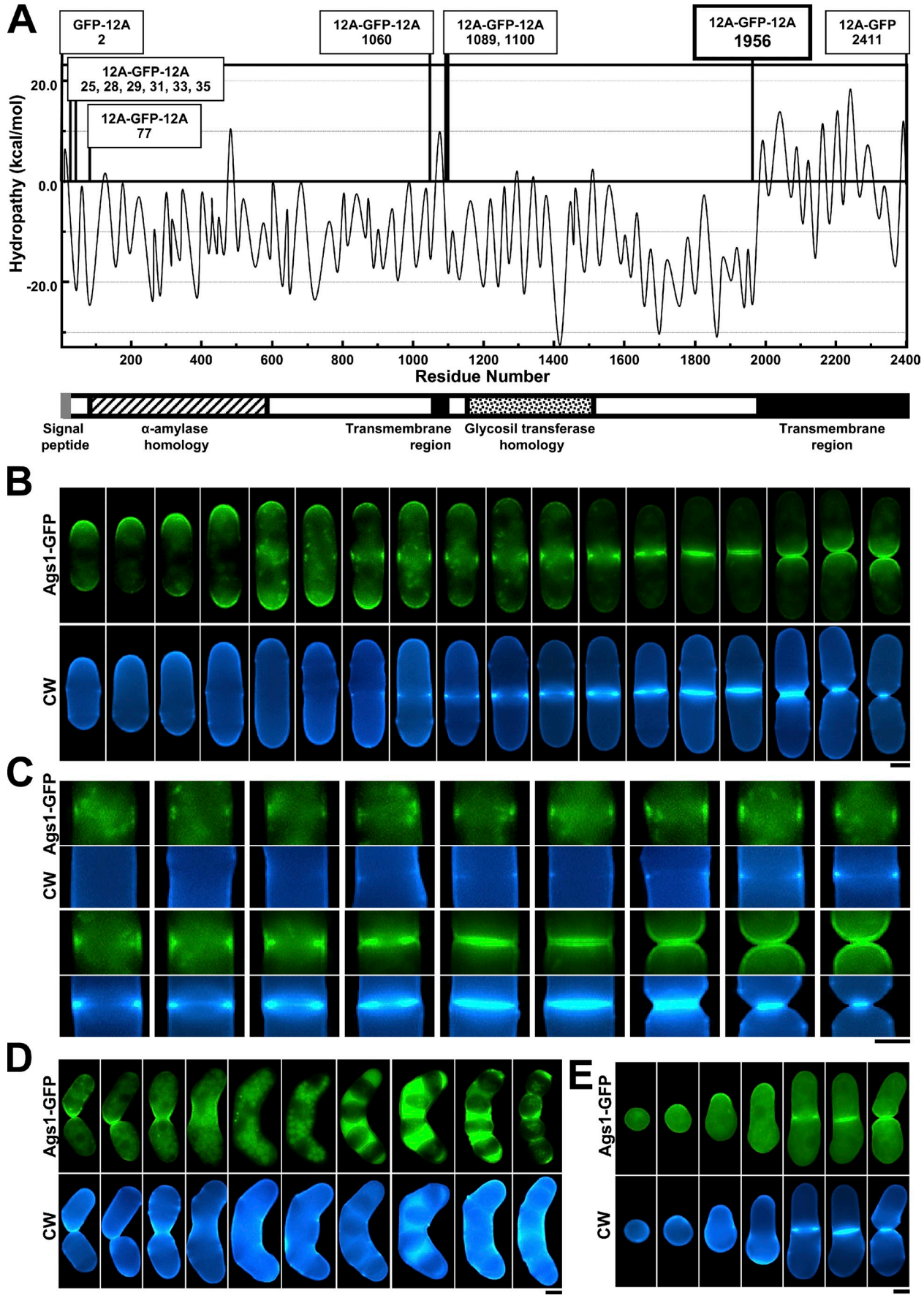

Published August 13, 2012

Ags1 (Mok1) is a putative α-glucan synthase (αGS) essential for cell integrity. Indirect immunofluorescence detected Ags1 in dividing and growing areas (Hochstenbach et al., 1998; Katayama et al., 1999). *S. pombe* contains four additional Ags1 homologues (Mok11–14), which are only detected during sporulation (García et al., 2006). αGS orthologues are not found in budding yeasts but are widely extended in pathogenic fungi (Edwards et al., 2011; Henry et al., 2012).

In this work, we have investigated the localization and requirements of Ags1 and found a tight colocalization with Bgs1, although they differ in their SIN dependence for medial positioning. We show for the first time that α(1-3)glucan is essential for both secondary septum formation and the primary septum robustness needed to support the turgor pressure during cell separation. Our findings bring to light convergent similarities between the primary septum α(1-3)glucan and the lamella pectin of plants, as both are essential for the adhesion and separation functions within similar structures.

Results

Ags1 localizes in the growing sites during vegetative and sexual phases

We examined the physiological localization of Ags1 by generating functional Ags1-GFP and -RFP fusions (Fig. 1 A, Fig. S1 A, and Materials and methods). During polar growth Ags1 was localized to the growing ends. Before the primary septum was detected, Ags1 simultaneously appeared in the growing ends and as a medial ring. After the primary septum was detected, Ags1 spread flanking the emerging septum and accumulating in the CAR. An obvious signal remained along the invaginated membrane, appearing as two separated bands after septum completion (Fig. 1, B and C; and Fig. S1 B).

Like the Bgs subunits, Ags1 was also present in all of the sites of wall synthesis during sexual differentiation: mating, spore formation, and spore germination (Fig. 1, D and E; and Fig. S1, D and E). These data suggest that Ags1 cooperates with the Ags1 homologues and Bgs proteins in cell fusion, spore wall formation, and spore germination.

Ags1 coincides spatially and temporally with Bgs1 in the growing sites: poles, CAR, and septum

As Ags1 and Bgs1 are the only GSs found in the medial region before the septum is detected, their localization and displacement from the tips to the CAR during mitosis was simultaneously analyzed. Time-lapse images showed that before the primary septum was detected (Fig. 2 A, arrow) Ags1 and Bgs1 colocalized as medial faint dots (Fig. 2 A, arrowhead). Furthermore, both Ags1 and Bgs1 concentrated in a ring that moved with the edge of the growing septum. However, the Ags1 signal remaining along the invaginated membrane was more intense than that of Bgs1 (Fig. 2 B and Fig. S1 C). During cell separation, Ags1 and Bgs1 remained at both sides of the degrading septum and moved simultaneously to the old end of each cell (Fig. 2 C).

We tested for a physical interaction finding that physiological Bgs1 and Ags1 coimmunoprecipitate (Fig. 2 E). This suggests either a physical interaction or the close presence of both proteins in the same plasma membrane domains.

Ags1 localization depends on the polarity establishment proteins, the polarized actin patches, and the polarized exocytosis

Ags1 localized to the poles during polar growth. *tea1-1* and *tea2-1* mutants fail to reinstate polarized growth along the long axis of the cell (Verde et al., 1995). In these mutants, Ags1 localized to the incorrect new growing tips (Fig. 3 A, left). On the contrary, the microtubule cytoskeleton was dispensable for the correct localization and displacement of Ags1 to poles and septum (Fig. 3 A, right and bottom).

Actin localization coincides with that of Ags1 throughout the cell cycle (Katayama et al., 1999). Therefore, we analyzed whether the actin cytoskeleton is involved in the correct Ags1 localization. In the actin mutant *cps8-188* the actin patches appeared depolarized (Ishiguro and Kobayashi, 1996), and Ags1 extended from the septum and poles along the plasma membrane all around the cell (Fig. 3 B, left). In contrast, polymerized F-actin was unnecessary for stable Ags1 localization in growing sites (Fig. 3 B, middle).

Formin For3 and type V myosin Myo52 are responsible for polarized actin cable assembly and transport of cargoes along the actin cables, respectively (Feierbach and Chang, 2001; Win et al., 2001). In the absence of For3 or Myo52, Ags1 localized correctly to the growing poles and septum (Fig. 3 B, right). These findings are in agreement with the fact that loss of function of profilin Cdc3, essential for actin cable formation (Balasubramanian et al., 1994), still permitted polarized growth and localization of Ags1 in cell tips (Fig. 3 B, bottom).

The exocyst is essential for polarized fusion of secretory vesicles with the plasma membrane (Wang et al., 2002). In the exocyst mutant *sec8-1*, Ags1 accumulated in the surrounding areas of tips and septa but no signal was detected in the plasma membrane (Fig. 3 C). Thus, Ags1 localization to regions of active cell wall synthesis depends on the correct actin patch localization and the polarized exocytosis.

Ags1 localization in the division site depends on the CAR formation and positioning, but not on the SIN pathway

To study the Ags1 requirements during septation, Ags1 localization in mutants affected in CAR positioning and formation was analyzed. In *mid1* mutants (Chang et al., 1996), CAR and

Figure 1. **Ags1 localizes in the growing sites during vegetative and sexual phases.** (A) Predicted Ags1 topology and tested GFP insertions to obtain a functional Ags1-GFP (see Materials and methods). (B) Physiological Ags1-GFP localization throughout the cell cycle. (C) Magnification of Ags1-GFP localization in the CAR and septum membrane. (D and E) Ags1 is localized to all sites of wall synthesis during sexual differentiation (D) and spore germination (E). h90 *ags1*$^{+}$*-GFP* cells were grown to early stationary phase and transferred onto SPA plates. (D) Samples were collected after 3, 5, 8, 24, and 48 h and examined. (E) Spores were collected after 10 d and incubated in YES medium. Samples were taken after 2 to 11 h. Bars, 2.5 µm.

Published August 13, 2012

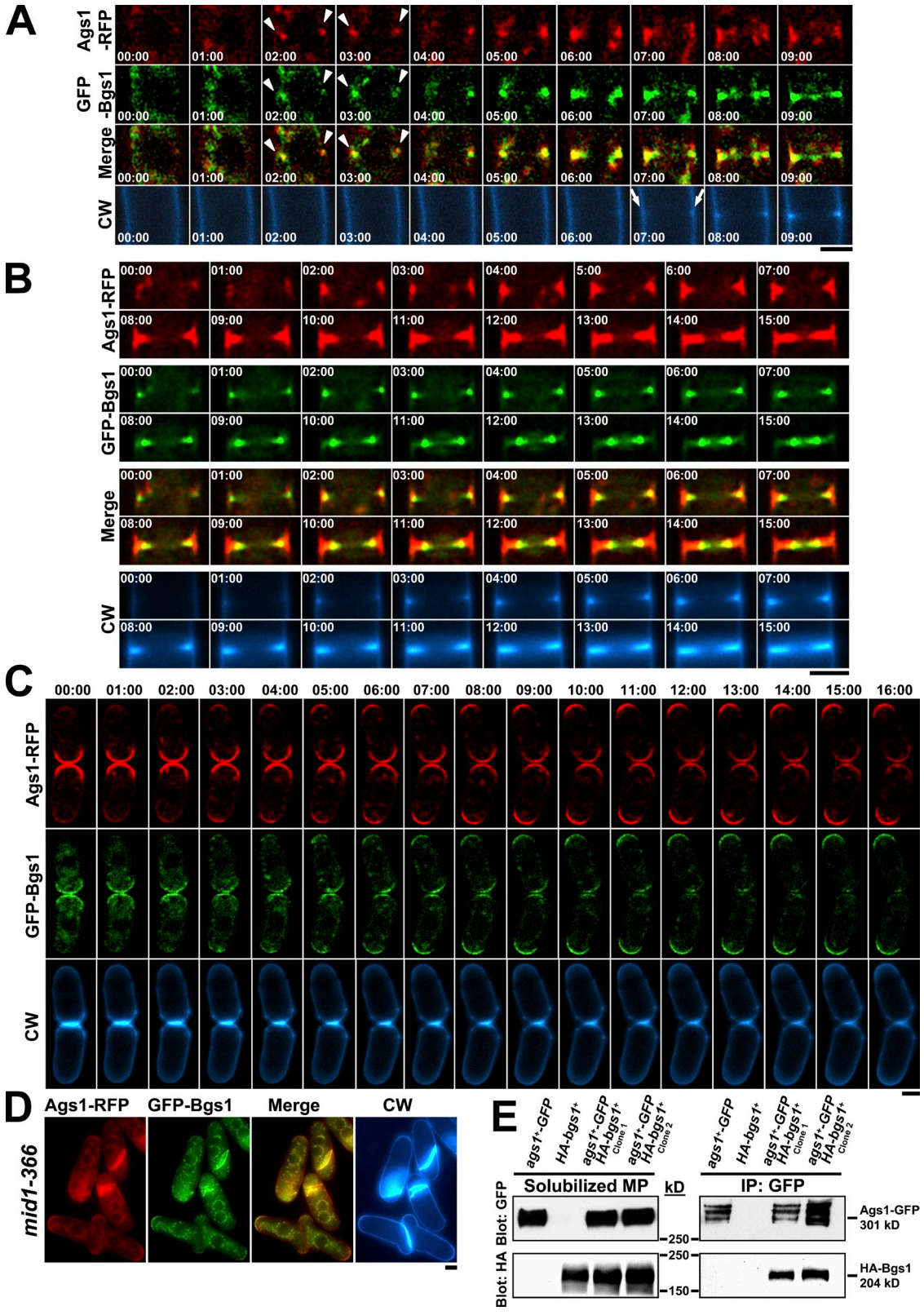

Figure 2. **Ags1 coincides spatially and temporally with Bgs1 in the growing sites: CAR, septum, and poles.** (A) Ags1 and Bgs1 colocalize in the medial zone before septum synthesis. *ags1⁺-RFP GFP-bgs1⁺* cells were imaged by time-lapse microscopy. Arrowhead: appearance of Ags1 and Bgs1 in the cell middle; arrow: appearance of septum (CW staining). (B) Ags1 and Bgs1 colocalize in the CAR and septum membrane. (C) Ags1 and Bgs1 colocalize in the old end before cytokinesis completion. Elapsed time is shown in minutes. (D) Ags1 and Bgs1 colocalize in the aberrant septa of the medial ring mutants. *mid1-366 ags1⁺-RFP GFP-bgs1⁺* cells were shifted to 32°C for 6 h. (E) Bgs1 coimmunoprecipitates with Ags1. Solubilized membrane proteins (MP; see Materials and methods) from the indicated strains were immunoprecipitated (IP) with anti-GFP serum. Solubilized MP (left) and IP (right) were transferred to the same membrane and blotted with monoclonal anti-GFP or anti-HA antibodies. Bars, 2.5 µm.

Published August 13, 2012

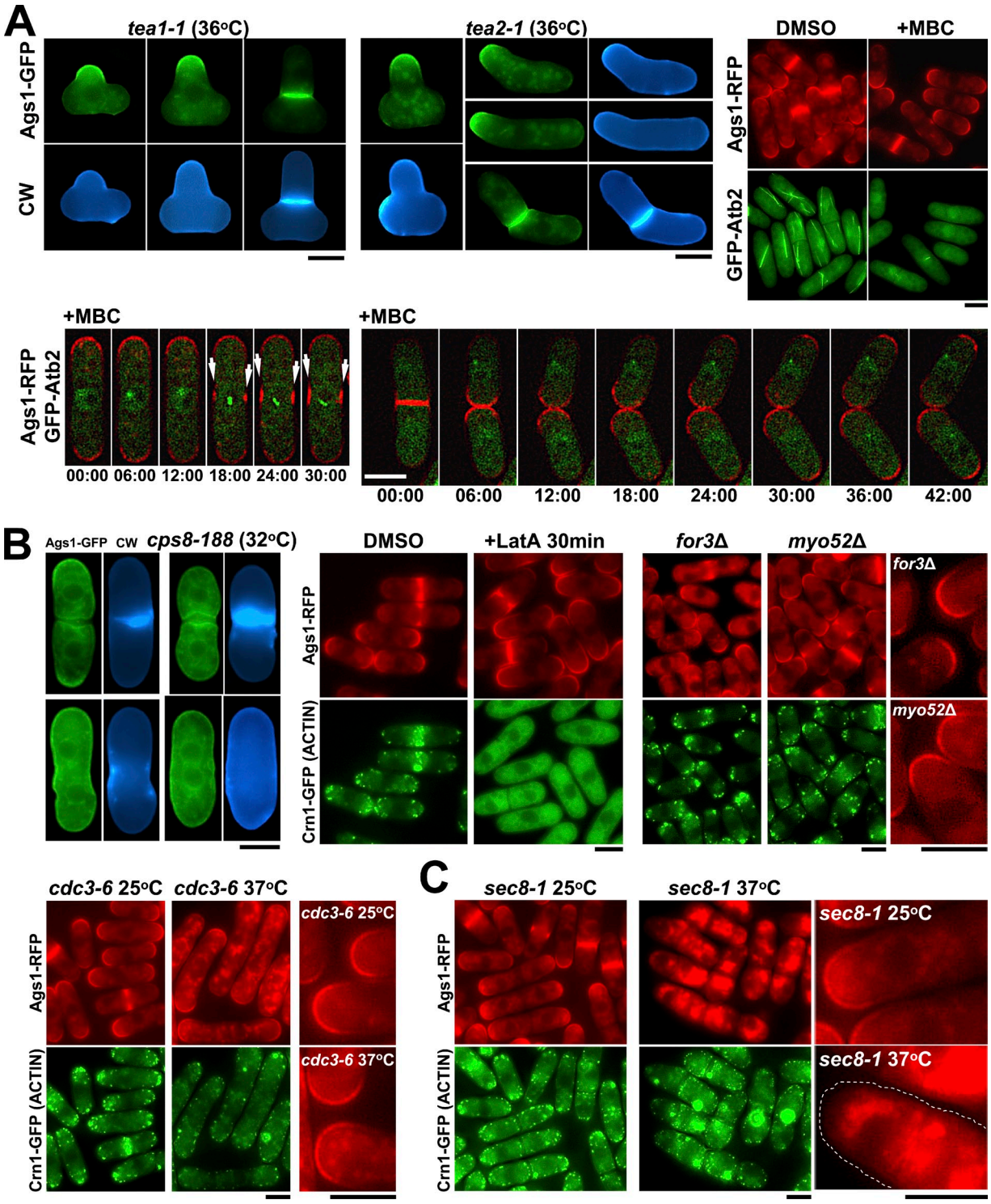

Figure 3. **Ags1 localization depends on the polarity establishment proteins, polarized actin patches, and polarized exocytosis.** (A) Ags1 localization depends on the polarity proteins but not on the microtubule cytoskeleton. Left: *ags1⁺-GFP* mutant cells were shifted to 36°C for 6 h. Right and bottom: *ags1⁺-RFP GFP-atb2⁺* cells were transferred to medium containing 25 µg/ml MBC for 30 min and imaged. Arrow: Ags1 displacement to the middle of the cell. Elapsed time is shown in minutes. (B) Ags1 localization depends on the correct actin patch polarization, but not on the polymerized actin, actin cables, and type V myosins. Left: *cps8-188 ags1⁺-GFP* cells were shifted to 32°C for 4 h. Middle: *ags1⁺-RFP crn1⁺-GFP* cells were transferred to medium containing 100 µM Lat A for 30 min. Right and bottom: *ags1⁺-RFP crn1⁺-GFP* mutant cells were grown at 28°C (*for3*Δ and *myo52*Δ) or at 25°C and shifted to 37°C for 2 h (*cdc3-6*). (C) Ags1 localization depends on the exocytosis. *sec8-1 ags1⁺-GFP* cells were shifted to 37°C for 2 h. Bars, 5 µm.

primary septum are positioned at arbitrary sites, always coincident with Bgs1, but not with Bgs4 (Cortés et al., 2005). In the *mid1-366* mutant, Ags1 was always coincident with septum alterations and Bgs1 localization (Fig. 2 D).

In the CAR formation mutants (Balasubramanian et al., 1994; Fankhauser et al., 1995) Ags1 was detected at cell poles and/or coincident with the incorrect septum structures (Fig. 4 A and unpublished data). The F-Bar protein Cdc15 is essential for

Published August 13, 2012

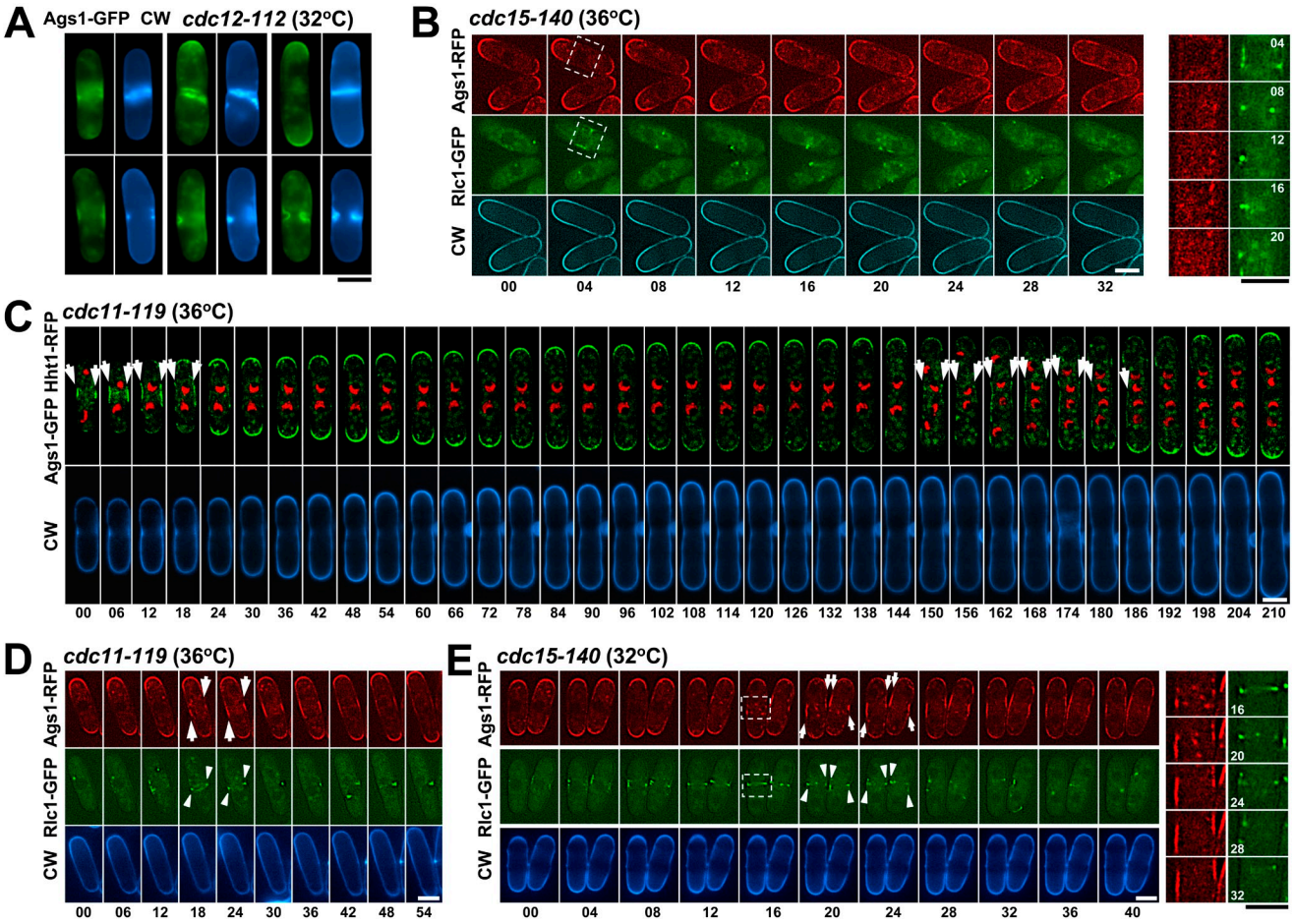

Figure 4. **Ags1 localization in the division site depends on the CAR formation, but not on the SIN pathway.** (A) *cdc12-112 ags1⁺-GFP* cells were shifted to 32°C for 4 h. (B) *cdc15-140 ags1⁺-RFP rlc1⁺-GFP* cells were shifted to 36°C for 30 min and imaged by time lapse. (C) *cdc11-119 ags1⁺-RFP rlc1⁺-GFP* and (D) *cdc11-119 ags1⁺-GFP hht1⁺-RFP* cells were shifted to 36°C for 1 h. (E) *cdc15-140 ags1⁺-RFP rlc1⁺-GFP* cells were shifted to 32°C for 30 min. Square: magnified area. Arrow: Ags1 localization in the medial region. Arrowhead: unstable CAR appearance in the middle of the cell. Elapsed time is shown in minutes. Bars, 5 µm.

CAR maturation. The *cdc15-140* mutant does not form aberrant septum structures but generates an unstable CAR that rapidly disappears (Hachet and Simanis, 2008). To know whether this defective CAR is sufficient for a transient Ags1 localization to the cell middle, time-lapse of *cdc15-140* cells at restrictive temperature and expressing both Ags1-RFP and Rlc1-GFP (CAR labeling) was performed (Fig. 4 B). In these cells Ags1 was never detected in the medial cortex, indicating that a stable CAR is essential for Ags1 localization in the division site.

The SIN is a signaling network required for CAR contraction and septum formation in *S. pombe* (Barral and Liakopoulos, 2009). Thus, we examined whether Ags1 medial localization depends on the SIN. The SIN mutants suffer a cytokinesis blockage after mitosis, building a CAR that disassembles prematurely rather than undergoing constriction and septum synthesis (Sparks et al., 1999; Krapp et al., 2001; Rosenberg et al., 2006). In these mutants, Ags1 localized to the poles and as a broad band in the cell middle (Fig. S2 A, arrow; and unpublished data), indicating that the SIN is not necessary for Ags1 displacement to the middle during cytokinesis.

To know if the Ags1 medial localization in SIN mutants occurs specifically during mitosis and during or after CAR presence, time-lapses of SIN mutants expressing both Ags1-GFP and Hht1-RFP (nucleus labeling) or Ags1-RFP and Rlc1-GFP were performed. During mitosis and after CAR assembly (Fig. 4 D, arrowhead) Ags1 disappeared from the tips and concentrated in the cell cortex surrounding the CAR and the mitotic nuclei. However, Ags1 never became concentrated as a ring structure; instead, it spread as a broad band as CAR collapsed (Fig. 4, C and D, arrow; and Fig. S2 B). When the nuclei were closely paired and the cell reinitiated bipolar growth, Ags1 moved to both cell tips. Similar Ags1 medial localization and dynamics were observed during the second round of mitosis (Fig. 4 C, arrow).

Occasionally some SIN mutant cells maintained the CAR longer, and in this case Ags1 concentrated as a ring overlapping the CAR that was able to constrict, giving rise to CW-stained septum structures (Fig. S2, C and D [Ags1, arrow; CW, arrowhead). Interestingly, the emergence of these septum structures frequently coincided with cell death before growth reinitiation, but never with septum completion.

In agreement with the SIN dependence of Cdc15 recruitment to the CAR, the *cdc15-140* mutant shows a similar cytokinesis

Published August 13, 2012

phenotype to that of SIN mutants (Hachet and Simanis, 2008). However, Ags1 did not localize in the cell middle of *cdc15-140* cells grown at a restrictive temperature (Fig. 4 B and unpublished data). Thus, time-lapse of *cdc15-140* cells growing at low restrictive temperature was performed. The *cdc15-140* cells displayed a more stable and uniform CAR that still disassembled prematurely (Fig. 4 E, arrowhead). In this case and like in SIN mutants, Ags1 appeared in the medial site and spread along the cell cortex as CAR collapsed (Fig. 4 E, arrow). These observations indicate that Ags1 displacement to the cell middle depends on a stable CAR, whereas the SIN signaling is exclusively needed for Ags1 localization in a ring structure.

Ags1 is essential for the septum integrity at the start of cell separation

To study the lethal effect of the absence of Ags1, a strain expressing a single integrated *ags1*$^+$ copy under the control of the thiamine-repressible 81X-*nmt1*$^+$ promoter was analyzed (see Materials and methods). Cell growth arrested after 4 h of *ags1*$^+$ repression and osmotic stabilization protected the cells, delaying the growth arrest to at least 12 h (Fig. 5 A, left). Morphological observations revealed that Ags1 depletion promotes cell lysis and cytoplasm release from the lateral region of the poles (Fig. 5 B, arrowhead) and mostly from the septum (Fig. 5 B, arrow). Total lysis reached 70% of the cells (n = 420) after 7 h of repression, and sorbitol reduced it to 7% (n = 986; Fig. 5 A, right). A similar lysis phenotype was observed in the *mok1-664* mutant at a restrictive temperature (Fig. 5 C). In agreement with previous data from *ags1*$^+$ point mutants (Hochstenbach et al., 1998; Katayama et al., 1999), the Ags1-depleted cells showed a considerable reduction (53%) in the cell wall α-glucan content (Table 1).

The septum lysis process of *ags1*$^+$-repressed cells was examined in detail by time-lapse (Fig. 5 D and Video 1). The lysis always appeared after septum completion, coincident with the start of cell separation. After 3 h of *ags1*$^+$ repression, lysis mostly occurred at the septum–cell wall border in only one cell (13% cells, n = 238; Fig. 5 D, top graph), generating one dead cell (arrowhead, top) attached to the living cell. After 7 h, lysis mostly occurred in both cells (41% cells, n = 420; Fig. 5 D, bottom graph) at both sides of the septum–cell wall border (arrowhead, bottom). Sorbitol delayed the cell lysis to 7 h. At this time most of the cells were still normal in growth and morphology (see graphs in Fig. 5, A and D).

Because Ags1 and Bgs1 might collaborate in the initial steps of septum formation, a possible genetic interaction was tested. Bgs1 and Ags1 interact genetically because the *cps1-12 mok1-664* mutant was more sensitive to temperature than the single mutants (Fig. S3 A). However, we found that the absence or defective function of Bgs1 (81X-*bgs1*$^+$ or *cps1-12* mutant) suppressed the lytic phenotype of either Ags1 absence or *mok1-664* mutation (Fig. S3 B). Interestingly, whereas *cps1-12* produced multi-septated cells, the *cps1-12 mok1-664* mutant arrested with no septa, suggesting collaboration between both proteins in septum and cell wall synthesis (Fig. S3 B). In agreement, the combined absence of both Bgs1 and Ags1 promoted strong cytokinesis defects not observed with Bgs1 absence alone (Fig. S3 B, arrow).

A possible genetic interaction between *ags1*$^+$ and SIN genes was also tested, finding that the *mok1-664* SIN double mutants are more sensitive to temperature than the single mutants (Fig. S3 A). The SIN mutants do not form septa, and therefore, the lysis of *mok1-664* mutant at the start of cell separation was abolished. Instead, a new and abundant lysis at the pole tip appeared (Fig. S3 C), indicating that Ags1 is also essential for cell wall integrity during polarized growth. In some cases, the SIN mutants lysed at the septum. This was due to the initiation of defective septa that cannot be completed. As expected, the *mok1-664* mutation increased the septum lysis defect of the SIN mutants (Fig. S3 C).

The absence of Ags1 alters the cell wall ultrastructure and leads to cell lysis at the lateral region of the poles

To further investigate the cell integrity defect caused by the absence of Ags1, the cell wall ultrastructure was examined (Fig. 6, A and C). The wild-type (WT) cell wall presented a three-layered structure (Fig. 6 A), whereas in the absence of Ags1 the cell wall became amorphous, thicker, and looser, with no signs of the outer dense layer. In the presence of sorbitol the wall appeared stratified with remedial internal dense and transparent layers (Fig. 6 A, ICW). This is in agreement with the different cell wall amounts detected with and without sorbitol. The cell wall increase detected with sorbitol was only due to β-glucan, suggesting a compensatory mechanism (Table 1).

The galactomannan has been detected in the outer and inner electron-dense layers (Horisberger and Rouvet-Vauthey, 1985). Because the outer layer was absent in Ags1-depleted cell walls, WT cells expressing Hht1-RFP (nuclear RFP) and *ags1*$^+$-repressed cells (no nuclear RFP) were mixed, stained with FITC-concanavalin A, and visualized for FITC and RFP (Fig. 6 B). Concanavalin A specifically binds to mannose residues, which can be used for indirect measurement of the mannan content and localization in the cell surface (Goldstein, 2002). Quantitative analysis of the FITC signal showed that in Ags1-depleted cells the outer galactomannan content was significantly reduced (Fig. 6 B), in agreement with the 36% decrease observed by cell wall fractionation (Table 1).

WT cells are surrounded by a uniform cell wall (Figs. 6 C and 7 A). In contrast, the cell wall of Ags1-depleted cells was irregular and displayed erosions in the pole lateral region (Fig. 6 C, open arrowhead; see also Fig. 9 C) and attached wall material from the sister cell (Fig. 6 C, closed arrowhead; see also Fig. 9 C).

The Ags1-depleted cells demonstrated cell lysis and cytoplasm release during polar growth. To study more precisely cell wall breakage, time-lapse of *ags1*$^+$-repressed cells was performed. Lysis always occurred not at the cell tip, but at the pole side region (Fig. 6 D, arrowhead). Lysis was detected at early repression times and increased during repression, reaching 8% of the cells at 7 h (n = 420; Fig. 6 D, graph). In the presence of sorbitol, lysis was delayed and reduced to 2% after 7 h of repression (n = 986; Fig. 6 D, graph). Interestingly, when the cells grown with sorbitol were imaged in the absence of sorbitol, the pole lateral lysis increased to 28% while the septum lysis remained in 6% (n = 453, not depicted).

Published August 13, 2012

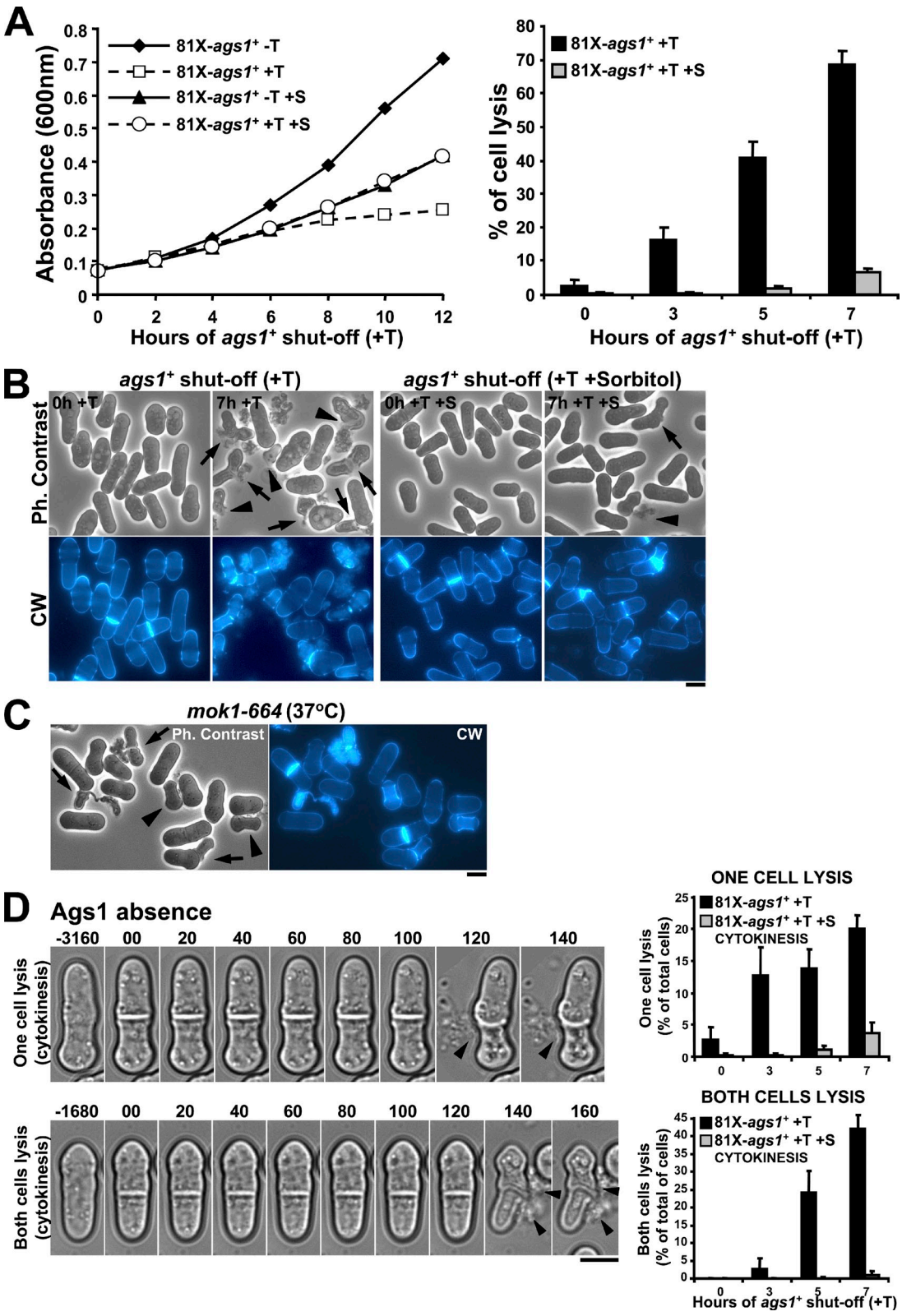

Figure 5. **Absence of Ags1 promotes cell lysis and release of cytoplasmic material from either the septum region or the lateral region of the pole.** (A) Sorbitol partially suppresses both cell growth arrest and cell lysis promoted by *ags1*$^+$ repression. 81X-*ags1*$^+$ cells were grown either without or with thiamine (−T, induced; +T, repressed) and 1.2 M sorbitol (S). Cell growth (left) and lysis (right) were monitored at the indicated times. (B) Absence of Ags1 promotes cell lysis at the septum and poles. Cells were grown as in A and visualized at the indicated times. (C) Loss of Ags1 function promotes similar cell lysis to that of Ags1 absence. *mok1-664* cells were grown in YES+S and shifted to 37°C for 5 h. Arrowhead: lysis in the pole side region; arrow: lysis in the septum region. (D) *ags1*$^+$ repression promotes cell lysis and release of cytoplasm from the division site, at the start of cell separation, resulting in the death of either one (top panels) or both sister cells (bottom panels). 81X-*ags1*$^+$ cells were grown in EMM+T for 3 h and visualized by time lapse. Arrowhead: lysed cell. Elapsed time is shown in seconds. The percentage of each cell lysis was quantified. Bars, 5 µm.

Published August 13, 2012

Table 1. **Incorporation of [^{14}C]glucose into cell wall polysaccharides during Ags1 depletion either in the absence or presence of 1.2 M sorbitol**

Growth	Strain	Thiamine[a]	% Incorporation of [^{14}C]glucose[b]			
			Cell wall	α-Glucan	β-Glucan	Galactomannan
EMM	Control	− (on, wt)	28.1 ± 2.8 (100)[c]	5.5 ± 0.3 (19.8)	19.2 ± 1.6 (68.5)	3.3 ± 0.8 (11.7)
EMM	81X-*ags1*$^+$	+ (off)	21.2 ± 0.7 (100)	2.6 ± 0.1 (12.1)	16.5 ± 1.2 (77.8)	2.1 ± 0.6 (10.1)
EMM+S	Control	− (on, wt)	26.8 ± 3.0 (100)	5.3 ± 1.0 (19.9)	17.9 ± 1.3 (66.9)	3.6 ± 0.8 (13.2)
EMM+S	81X-*ags1*$^+$	+ (off)	32.0 ± 2.7 (100)	3.4 ± 0.6 (10.9)	25.0 ± 3.2 (77.7)	3.6 ± 0.5 (11.4)

[a]*ags1*$^+$-repressed cell cultures were grown for 3 (EMM) or 7 h (EMM+S) in the presence of thiamine. [^{14}C]glucose was added 1.5 or 4 h before harvesting, respectively. S, 1.2 M sorbitol.
[b]Percent incorporation of [^{14}C]glucose = cpm incorporated per fraction × 100/total cpm incorporated. Values are the means and SDs calculated from three independent experiments.
[c]Values are percentages of the corresponding polysaccharide in the cell. Values in parentheses are percentages of the polysaccharide in the cell wall.

These data indicate that Ags1 and the corresponding α(1-3)glucan are essential to maintain cell wall structure and integrity during cell growth.

Ags1 is responsible for both secondary septum synthesis and correct primary septum formation

To study in more detail the role of Ags1 in septum synthesis, the septum ultrastructure of Ags1-depleted cells was analyzed. WT cells presented a three-layered septum structure (Fig. 7 A). As the primary septum grew, the secondary septum was laid down at both sides. After septum closure, the septum thickness increased in a maturation process involving additional secondary septum synthesis. The final septum displayed a primary septum invading the cell wall (arrow) and flanked by two triangular electron-dense structures termed "materiel triangulaire dense" (MTD; Johnson et al., 1973; Fig. 7 A, bottom).

The Ags1-depleted cells presented strong septum defects of abruptly twisted (Fig. 7, B–D) and not anchored primary septa (arrow) and disorganized MTD structures (Fig. 7, C and D). This indicates that Ags1 is essential for a straight primary septum synthesis, and suggests an important Ags1 cooperation with Bgs1 and the CAR. In addition, Ags1 is also essential for primary septum anchorage and MTD assembly. Sorbitol delayed the lytic phenotype, revealing a primary septum synthesized with no secondary septum (Fig. 7 C). At longer repression times, a new remedial internal cell wall (ICW) layer appeared (Figs. 6 A and 7 D). The primary septum could not drill the cell wall, but instead the base appeared anchored to the new ICW, which extended along the naked primary septum. This in turn gave rise to a new three-layered septum structure with a twisted primary septum flanked by remedial secondary septa (Fig. 7 D).

Ags1 is essential for the primary septum strength needed to support the cell separation internal pressure

The analysis of *ags1*$^+$-repressed cells showed that all of the cells separated asymmetrically and stayed coupled by their side (Fig. 8 A, arrowhead). Quantification showed that 21% of WT cells (n = 1,260) were in the separation process, which was straight and symmetrical (arrow). However, 41% of Ags1-depleted cells (n = 1,487) were in the separation process, which always was asymmetrical, or remained connected by their side after separation (Fig. 8 A, graph).

To further assess the nature of this defect, cell separation was monitored by time-lapse. WT cell separation was progressive and symmetrical (Video 2). The first step was a small symmetrical jump (t = 40; Fig. 8 B, Fig. S4 A, and Video 5) caused by the physical force of the turgor pressure after degradation of the septum edging. Next, progressive and symmetrical degradation of the primary septum was accompanied by a gradual curvature of the secondary septum to reach the most stable conformation in the new end.

Interestingly, cell separation in Ags1-depleted cells was instantaneous and asymmetrical, with a ripped primary septum, usually giving rise to one sister cell remaining attached to the well surface, and the other cell quickly jumping but staying connected by its side to the sister cell (Videos 3 and 4). This side-explosive phenotype was caused by asymmetrical degradation and/or breakage of the septum edging followed by an abrupt tear of a weak primary septum and an instantaneous curvature of the secondary septum (t = 20; Fig. 8 B, Fig. S4 B, and Videos 6–9). The secondary septum of WT cells needed 5 min from the separation start for a complete curvature, whereas in the absence of Ags1 this occurred in as much as 20 s (first captured image, asterisk, Fig. 8 B and Fig. S4 B). Cells imaged by normal microscopy showed that the abrupt primary septum tearing occurs in just the time spent between two image captures (1 s; Fig. 8 D). A similar side-explosive separation was observed in the *mok1-664* mutant (Fig. 8 C and Fig. S4 E).

After side-explosive separation, the sister cells remained attached by one side of the septum edging through remnants of a primary septum that was slowly degraded (Fig. 8 E). Importantly, the new end of both sister cells displayed considerable amounts of primary septum remnants, indicating that the immediate cell separation is caused by a fast internal tear of a weak primary septum that cannot withstand the cell pressure that curves the secondary septum (Fig. 8 E). This shows that the α(1-3) glucan forms part of the primary septum and is essential to confer it the strength needed to support the cell internal pressure during cell separation.

We examined if the primary septum weakness also affected its linkage to the secondary septum, resulting in cell separation through not only internal tearing but also in the primary–secondary septum boundary. As expected, all the *ags1*$^+$-repressed (n = 612) and *mok1-664* cells (n = 358) separated asymmetrically.

Published August 13, 2012

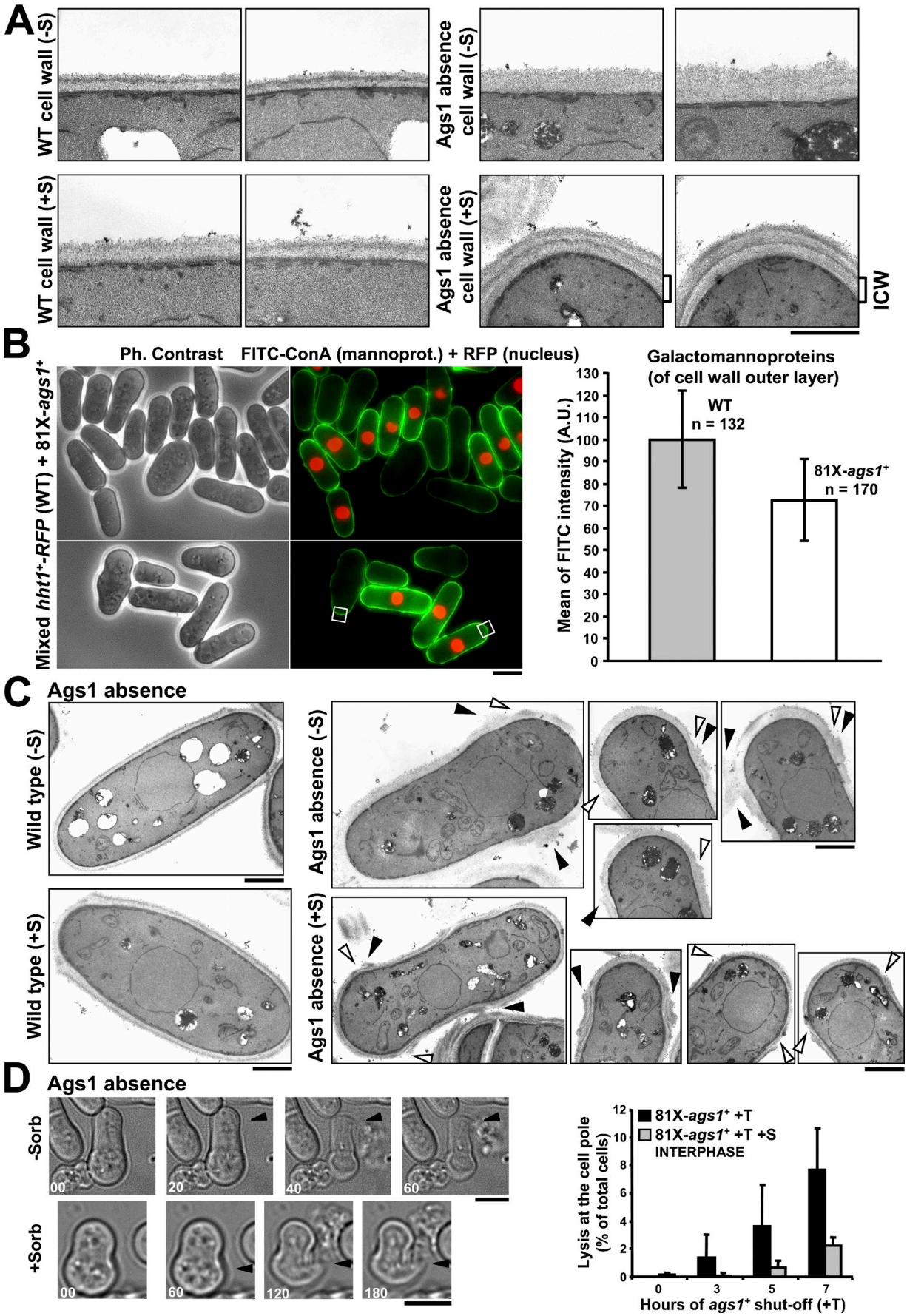

Published August 13, 2012

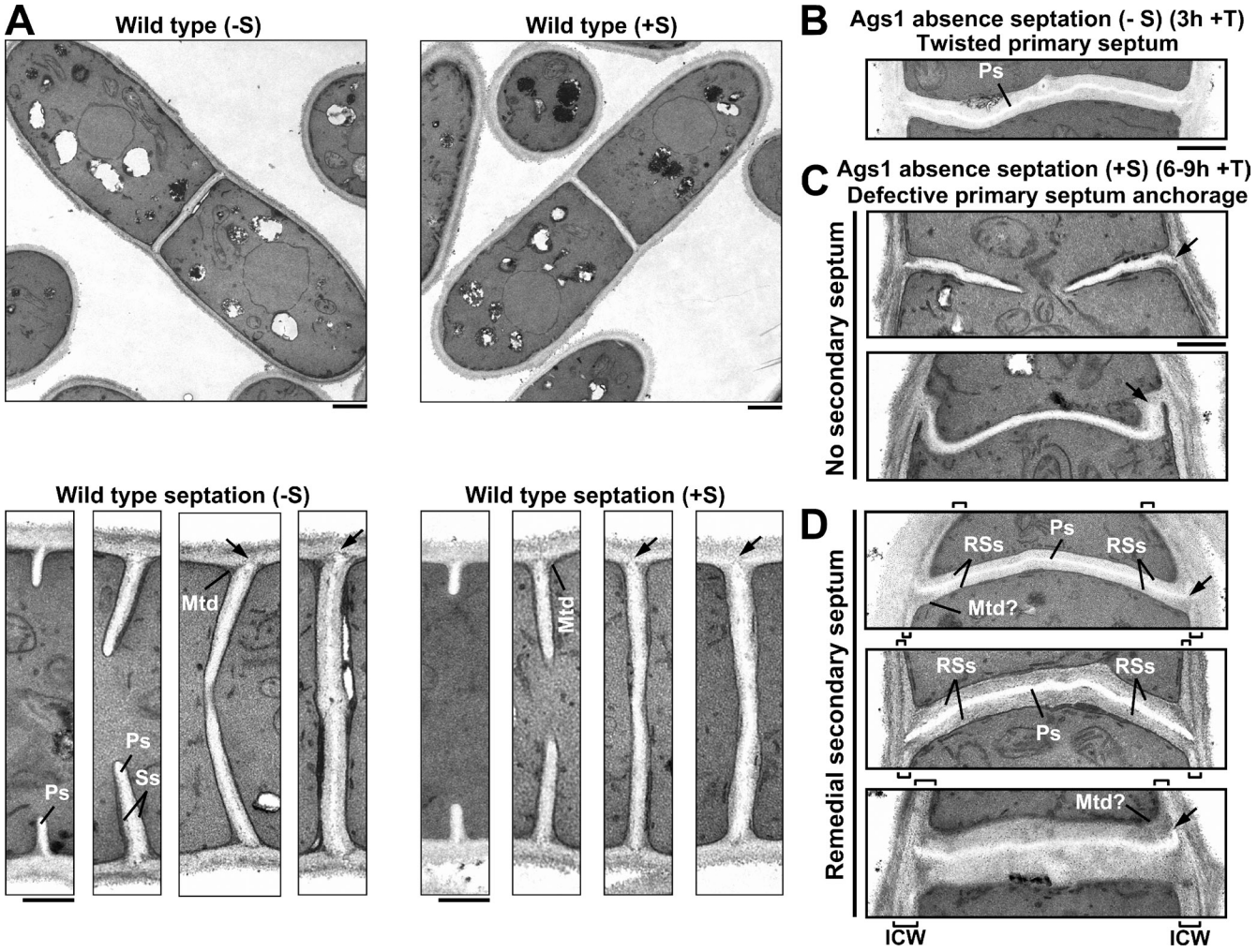

Figure 7. **Ags1 is responsible for the secondary septum formation and the correct primary septum structure.** (A) WT cell morphology and septum formation details. (B–D) Absence of Ags1 generates (B) twisted primary septa, (C) septa with no secondary septum, and (D) a remedial internal cell wall and secondary septum layer. Cells were grown in EMM+T for 3 (−S) or 6–9 h (+S) and analyzed by TEM. ICW, internal cell wall; Mtd, materiel triangulaire dense; Mtd?, diffuse Mtd; Ps, primary septum; RSs, remedial secondary septum; Ss, secondary septum; arrow, primary septum end anchoring (WT) or defective anchoring (Ags1 absence) into the cell wall. Bars: (WT, top) 1 µm; (rest of panels) 0.5 µm.

Depending on the localization of primary septum remnants (Fig. S4, D and E, arrow), three types of paired cells were detected: (1) both new ends exhibiting CW-stained material, indicating an internal primary septum tearing; (2) only one new end presenting CW-stained material, suggesting a tearing through the contact region between primary and secondary septum; and (3) in later separation stages, the new ends did not display detectable CW-stained material, but the cells were still firmly connected through a small cell wall area with little or no CW staining (Fig. 9 A and Fig. S4 E, circle).

The absence of Ags1 causes a final cell separation defect

Only primary septum CW staining ensures that two cells closely observed by microscopy are physically attached. In Ags1-depleted cells, the CW staining of the side-contact region eventually disappeared. However, many cells appeared in close lateral contact (Figs. 8 A and 9A), suggesting that they remain attached by their side. To find out how and when the side-contact region is degraded to complete cell separation, time-lapse of paired Ags1-depleted cells connected by their side region was

Figure 6. **Absence of Ags1 alters the cell wall structure and composition and causes a lack of cell wall in the pole lateral region, which leads to lysis and cytoplasm release.** (A) Ags1 depletion promotes general cell wall ultrastructure alterations, thicker and uniformly transparent in the absence (top-right panels) or multilayered in the presence of sorbitol (bottom-right panels). Cells were grown in EMM+T for 3 (−S, top panels) or 9 h (+S, bottom panels) and analyzed by transmission electron microscopy (TEM). ICW: internal cell wall layer. Bar, 1 µm. (B) Absence of Ags1 generates a reduction in the outer layer of mannoproteins. *hht1⁺-RFP* (WT, RFP nuclei) and 81X-*ags1⁺* (no RFP nuclei) cells were grown in EMM+T for 3 h, mixed, and visualized for FITC-concanavalin A (mannoproteins) and RFP fluorescence (nuclei, WT cells). FITC fluorescence (mannoproteins amount) was quantified by using arbitrary units (see Materials and methods). Bar, 5 µm. (C) Ags1 depletion causes irregular walls with cavities (open arrowhead) and/or attached sister wall fragments (closed arrowhead) at the pole side region. Cells were analyzed by TEM as in A. Bars, 1 µm. (D) Ags1 depletion promotes lysis and cytoplasm release from the pole side region. Cells were grown as in A. Arrowhead: lateral region of cell lysis. Elapsed time is shown in seconds. The percentage of lateral lysis was quantified. Bars, 5 µm.

Published August 13, 2012

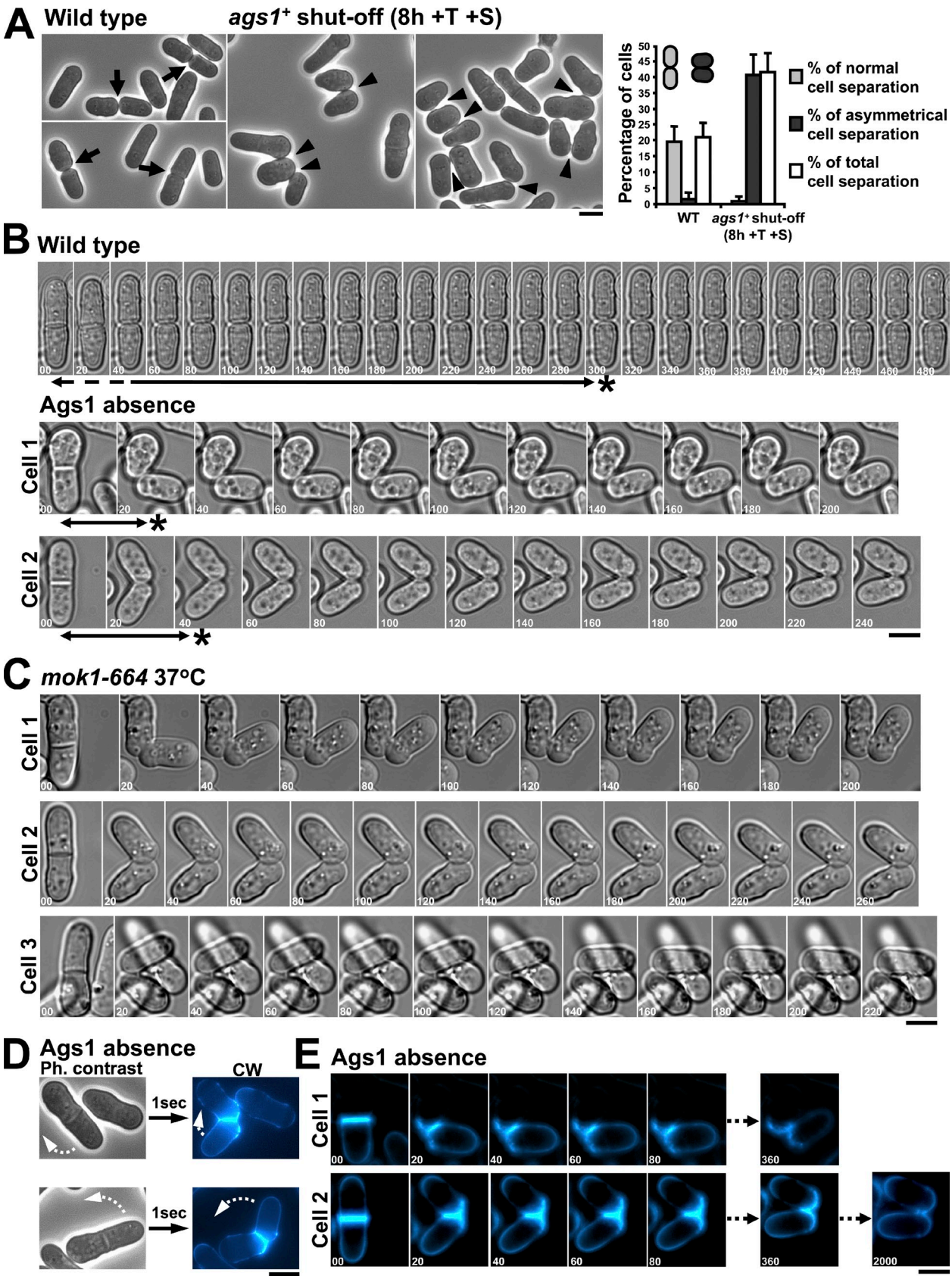

Figure 8. **Ags1 is responsible for the strength of the primary septum structure needed during cell separation.** (A) Ags1-depleted cells exclusively display asymmetrical cell separation and remain attached by their side. Arrow: normal straight separation; arrowhead: asymmetrical separation. Cells were grown in EMM+T+S for 8 h. The percentage of each cell separation was quantified. (B) WT cells separate gradually (top panels), whereas the Ags1-depleted cells suffer an immediate side-explosive separation. Cells were grown in EMM+T for 3 h and imaged. Asterisk, time spent for maximal new end curvature.

Published August 13, 2012

performed (Fig. 9 B, arrowhead). After 240 min the cells still remained connected (arrowhead), each already containing a new septum ready to be ripped. In this example, the side-explosive separation of the new septum (Fig. 9 B, a1–a2) released the connected cells from the well surface (path shown by broken arrow). In other cases, the side-explosive separation did not necessarily cause detachment from the surface (Video 1). During movement, the cells still stayed connected through the initial side-contact region (Fig. 9 B, arrowhead, a1–b1, t = 237:40 to 255:00; and Video 10). Under our time-lapse conditions, the cells stayed connected for more than one cell cycle, whereas in shaking cultures only paired cells were detected. This result suggests that final cell separation of Ags1-depleted cells is a mechanical rather than enzymatic process.

Ultrastructure analysis of *ags1*$^+$-repressed cells confirmed the absence of degradation of the side-contact area maintaining both cells connected after separation (Fig. 9 C, arrow). This non-degraded area was located close to the fission scar, corresponding to the septum edging of the previous septum. The separated cells presented in the pole lateral region cavities and attached wall fragments (Fig. 9 C, open and closed arrowheads), suggesting a physical tear of the cell wall that connected both cells.

Discussion

In fungal cytokinesis, CAR contraction is intimately accompanied by centripetal assembly of a septum wall that physically separates the sister cells (Bathe and Chang, 2010). However, little is yet known about how the different essential GSs cooperate to assemble the septum structures. Once septation is accomplished, subsequent cell separation requires the selective degradation of the primary septum (Sipiczki, 2007). Because of the high turgor pressure, even a minor rupture of the cell wall structure might conduct to lysis and cell death. Therefore, correct assembly and structural integrity of the cell wall and specialized septum are vital for cell survival (Cabib et al., 2001).

S. pombe is an attractive model for morphogenesis whose growth pattern likely diverged from filamentous fungi in response to the loss of hyphal growth (Harris, 2011). Like fission yeast, the cell wall of filamentous fungi also contains β- and α-glucans (Latgé, 2007). *S. pombe* IEM studies allowed the localization of the β-glucans in specific sites of cell wall and septum (Humbel et al., 2001; Cortés et al., 2007). To date, the cell wall α(1-3)glucan distribution and function is unknown (Sugawara et al., 2003; Grün et al., 2005). Ags1 was described as a putative αGS essential for cell integrity, but a specific role for Ags1 in the cell wall and septum architecture has not yet been described (Hochstenbach et al., 1998; Katayama et al., 1999).

We succeeded in generating a fully functional Ags1-GFP, and interestingly, Ags1 localizes very early in division sites and poles, coinciding exactly with Bgs1. Both Ags1 and Bgs1 localize before and ahead of the growing primary septum. Ags1 and Bgs1, but not Bgs4, overlap with the aberrant CW-stained septum material of the CAR positioning mutant *mid1-366*. Importantly, Bgs1 coimmunoprecipitates with Ags1, and *ags1*$^+$ and *bgs1*$^+$ interact genetically, suggesting a tight cooperation between both GSs in primary septum assembly. In fact, Bgs1 depletion produces septa with no primary septum but still containing diffuse L-BG, suggesting that L-BG association with branched β(1-3) and/or α(1-3)glucan is critical for primary septum assembly (Cortés et al., 2007).

Independently of the close Ags1–Bgs1 cooperation and although both are GSs, Ags1 is structurally very distinct and presents a relevant difference with the Bgs family with respect to their dependence on the SIN for medial localization (Cortés et al., 2005), indicating different requirements for medial localization and/or activation. In the absence of a functional SIN, only Ags1 is able to localize in the division site during mitosis and in the presence of the CAR. In *cdc15-140* cells, Ags1 does not localize to the division site in the absence of the CAR and spreads along the medial cortex in the presence of a nonfunctional CAR, indicating that CAR serves as a landmark for Ags1 incorporation to the division site, whereas the SIN is exclusively involved in its ring localization and activation.

Ags1 α-glucan is essential for the primary septum strength needed during cell separation

S. pombe cell separation is the most critical step of the cell cycle, where the degrading primary septum must withstand the internal pressure and gradual secondary septum curvature to reach the most stable conformation in the new end. The normal septum structure is able to support the mechanical force of the internal pressure, allowing a symmetrical and progressive primary septum degradation and secondary septum curvature (Fig. 10 A). Our results show that Ags1 absence or loss of function generates a primary septum that is highly vulnerable to the separation internal pressure. After asymmetrical septum edging degradation, the primary septum is instantly torn by a side-explosive cell separation (Fig. 10 B), creating two sister cells with primary septum remnants in the new ends. These observations indicate that Ags1 synthesizes an α-glucan of the primary septum that is essential to confer it the mechanical strength needed to face the separation internal pressure.

In contrast to the chitinous primary septum of budding yeast, our data show that in addition to β-glucans, the primary septum of *S. pombe* also contains α-glucan. The primary septum is essential for *S. pombe* viability, whereas in *S. cerevisiae* it is dispensable. These differences might account for distinct division patterns and/or cell wall compositions: (i) *S. pombe* does not contain chitin, whereas the budding yeast primary septum is made of chitin. It seems reasonable to think that linkages between α- and

Broken arrow: first separation step of symmetrical cell wall degradation. (C) Loss of Ags1 function promotes a side-explosive separation similar to that of Ags1 absence. *mok1-664* cells were shifted to 37°C for 1 h and imaged. (D) The side-explosive cell separation (curved arrow) occurs instantly, in the interval between two image captures. Cells were grown as in A. (E) The side-explosive separation is caused by an abrupt primary septum tearing, which remains intact in the new poles for a long time. Cells from B were visualized by CW staining. Elapsed time is shown in seconds. Bars, 5 µm.

Published August 13, 2012

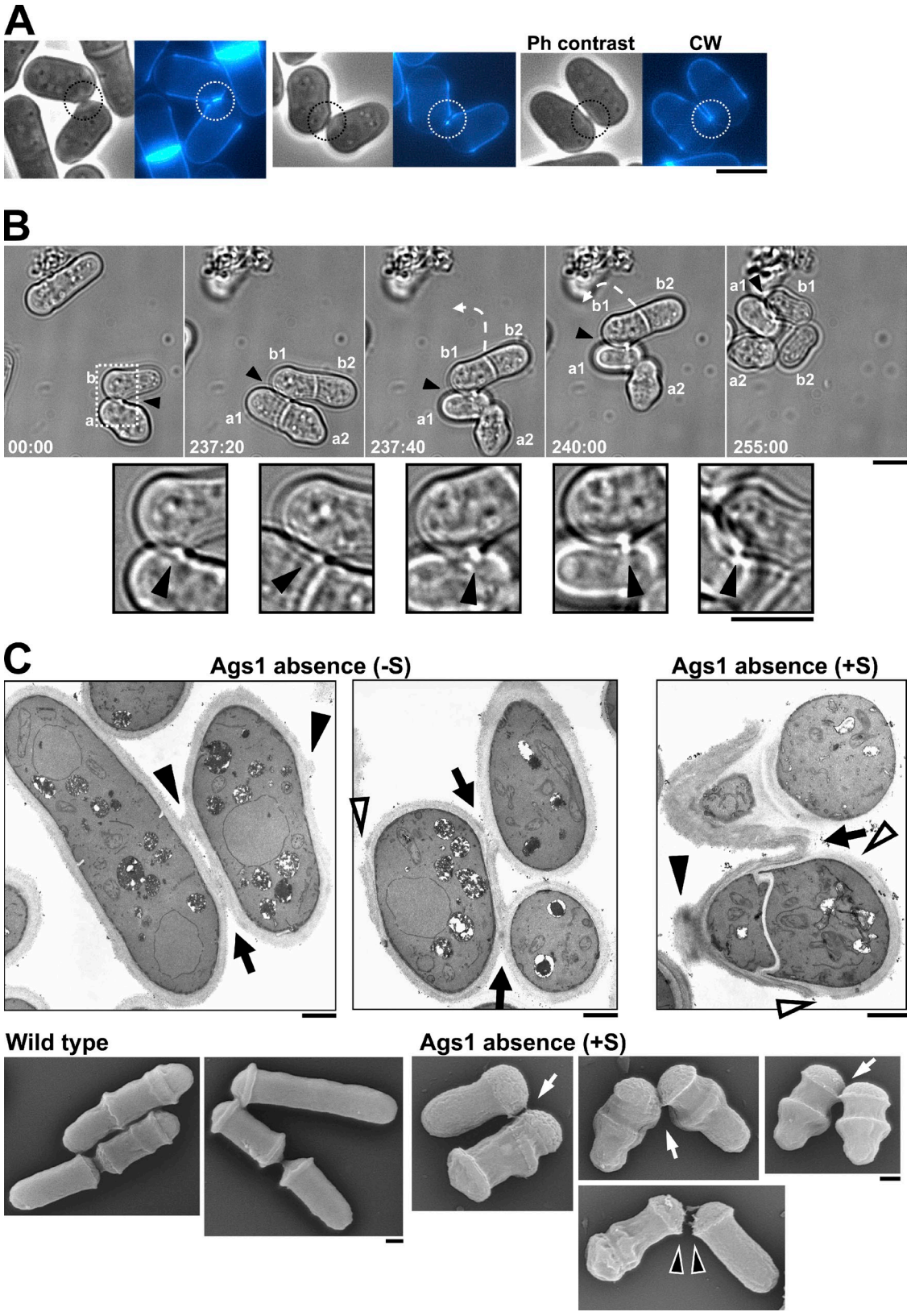

Figure 9. **Absence of Ags1 results in a defective final cell separation step.** (A) Ags1-depleted cells stay attached through the septum edging for a long time, even after disappearance of the remaining CW-stained primary septum. Cells were grown as in Fig. 8 A. Circle: side-contact region with different amounts of CW-stained primary septum. Bar, 5 µm. (B) The Ags1-depleted sister cells remain attached by their septum edging (arrowhead) for at least two cell cycles. Cells were grown in EMM+T+S for 4 h. Arrowhead: side-contact region. Broken arrow: movement of the attached cells. Square: magnified area. Elapsed time is shown in minutes. Bars, 5 µm. (C) Ultrastructure of Ags1-depleted cells attached by the septum edging (arrow). The cells display irregular walls with cavities (open arrowhead) and attached wall fragments (closed arrowhead) at the pole lateral region. Cells grown as in Fig. 6 A were analyzed by TEM (top) or scanning electron microscopy (SEM, bottom). Bars, 1 µm.

Published August 13, 2012

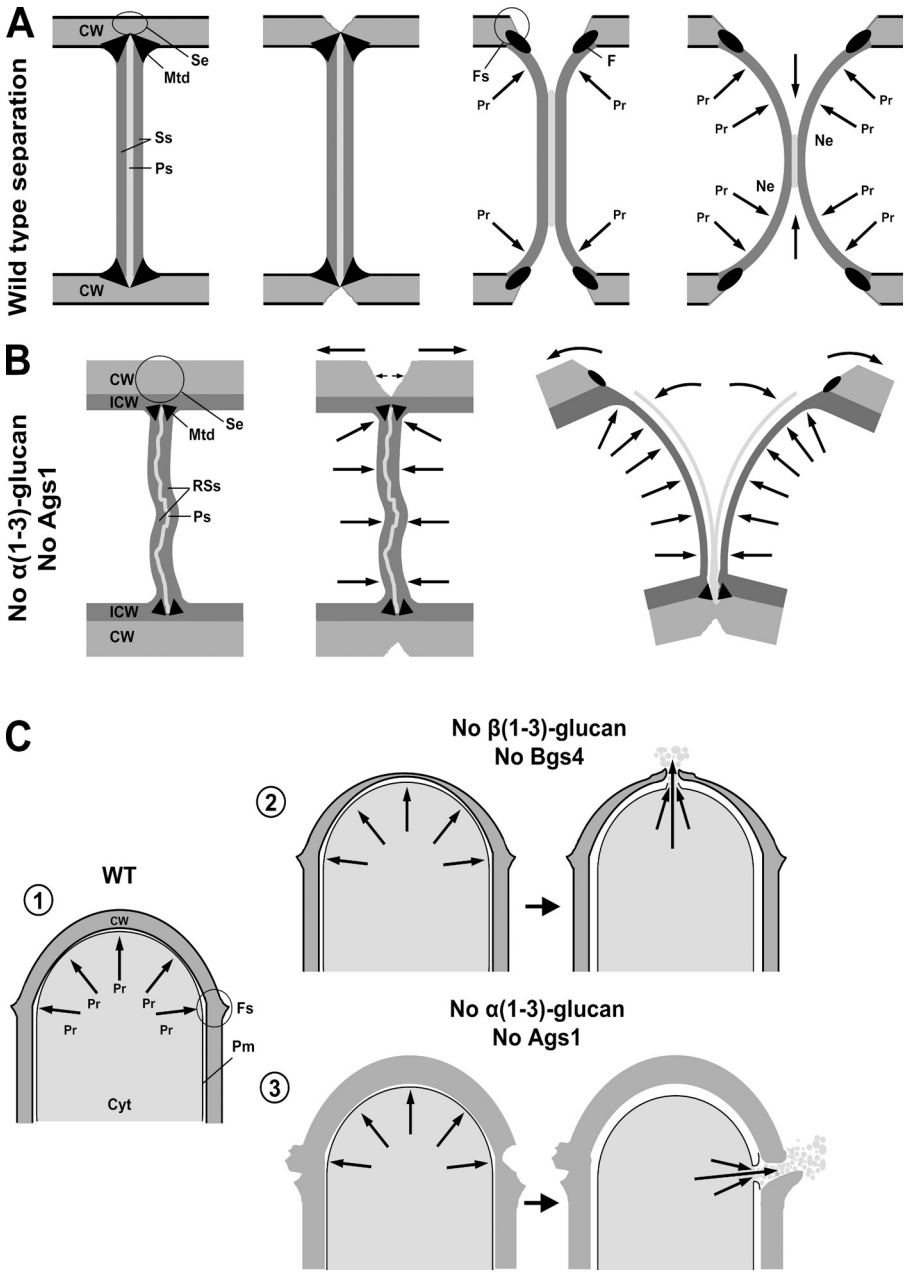

Figure 10. **Models of the septation apparatus and the apical growth of fission yeast.** (A) Septation and cell separation in WT cells. A balance between the osmotic pressure that curves the secondary septum to the stable spherical conformation and the degradation of the primary septum ensures a symmetrical and steady separation. (B) Alternative septation and side-explosive cell separation in the absence of Ags1 and the corresponding α-glucan. Asymmetrical septum edging degradation and mechanical tear of a weak primary septum that cannot hold the turgor pressure, leading to an instantaneous side-explosive separation to adopt the stable spherical conformation in both new ends. The cells stay attached by the septum edging for the next cell cycle. (C) Apical growth in WT and Bgs4- and Ags1-depleted cells. (1) The WT cell wall thickness is uniform, ensuring a balance between the turgor pressure and the strength of the growing cell wall. (2) Bgs4 absence produces a thin wall at the pole tip that cannot withstand the turgor pressure, leading to the wall rupture and cytoplasm release (unpublished data). (3) Ags1 absence causes wall cavities in the pole side region due to a defective final cell separation, leading to the cell lysis and cytoplasm release. CW, cell wall; Cyt, cytoplasm; F, fuscannel; Fs, fission scar; ICW, remedial internal cell wall layer; Mtd, materiel triangulaire dense; Ne, new end; Pr, turgor pressure; Pm, plasma membrane; Ps, primary septum; RSs, remedial secondary septum; Se, septum edging; Ss, secondary septum.

β-glucans would contribute to the mechanical strength of the primary septum. (ii) *S. pombe* primary and secondary septum assembly is simultaneous and closely coordinated, whereas the *S. cerevisiae* septum is synthesized sequentially. (iii) *S. pombe* septum covers the entire cell diameter, whereas in budding yeast it just closes the narrow mother-bud neck. (iv) *S. pombe* septum degradation gives rise to full-diameter new growth ends, whereas in *S. cerevisiae* it results in a small non-growing area. (v) *S. pombe* full-diameter septum degradation supports a considerable internal pressure, whereas in *S. cerevisiae* it must only support the pressure of the small disk area (Johnson et al., 1973; Schmidt et al., 2002; Cortés et al., 2007).

As we advance in our knowledge of fission yeast septation, we find new and surprising evolutionary convergent structural and functional similarities between fission yeast and plant septa: (i) as in *S. pombe*, the plant cell plate is made of callose (L-BG) and the protein involved is the Bgs homologue CalS1 (Verma and Hong, 2001; Cortés et al., 2007); (ii) *S. pombe* α-glucan and plant pectin (an α-linked polysaccharide) assume the same function in a similar structure. Both are essential for wall adhesion and safe cell separation, maintaining the linkages between polysaccharides in equivalent structures, the fission yeast primary septum and the plant mature cell plate (middle lamella; Iwai et al., 2002; Roberts and Gonzalez-Carranza, 2007).

Ags1 is responsible for secondary septum formation and cell wall integrity

Ags1 depletion generates fragile and twisted primary septa with no secondary septa, indicating that (i) Ags1 is responsible for the secondary septum assembly; and (ii) the perpendicular and straight primary septum deposition needs to be closely accompanied by a flanking secondary septum. Alternatively, the twisted

Published August 13, 2012

primary septum might be due to an essential Ags1 cooperation with Bgs1 and the CAR. Analysis of reverting protoplasts suggested that the primary cell wall formation step is the assembly of β-glucan microfibrils, whereas α-glucan might be involved in glucan bundle formation (Osumi et al., 1989; Konomi et al., 2003). Our results indicate that in the absence of α-glucan, the β-glucan microfibrils are unable to evolve into bundles, and therefore, the glucan network is not generated and the secondary septum is not assembled.

S. cerevisiae association between chitin and β(1-3)glucan grants to the wall the mechanical strength needed to withstand the internal pressure (Hartland et al., 1994). As *S. pombe* does not contain chitin, α- and β-glucans and their corresponding GSs have probably assumed multiple essential functions during cell wall synthesis, as is the case for the three chitin synthases in *S. cerevisiae* (Shaw et al., 1991). Our results show that Ags1 is also essential for cell wall integrity: (i) Ags1 localizes to the growing poles, suggesting that Ags1 synthesizes an α-glucan of the cell wall. (ii) Ags1 is essential for the correct cell wall architecture. In its absence the cell wall is amorphous, thicker, and looser, with no signs of the outer dense layer, reduced concanavalin A binding to the wall surface, and reduced cell wall galactomannan content. It is unknown how galactomannan is integrated into the cell wall, although our results suggest that part of the mannose residues might associate with the α-glucan fibrils. (iii) Ags1 depletion generates a predominant septum lysis at the start of cell separation, suggesting that Ags1 is essential to compensate an excess of cell wall degradation during separation. In addition to α-glucan, the secondary septum contains branched β(1-3)glucan. *bgs4*$^+$-repressed cells also display septum lysis at the beginning of cell separation (Cortés et al., 2005). Thus, it will be necessary to evaluate whether Bgs4 is responsible for the secondary septum β(1-3)glucan and how Ags1 and Bgs4 cooperate to assemble this structure.

Ags1 and Bgs4 are also essential for cell integrity during apical growth, although by different mechanisms (Fig. 10 C). Bgs4 absence generates a thin-tip cell wall leading to lysis at the pole tip (unpublished data). However, Ags1 absence produces lysis at the pole lateral region. Interestingly, the pole lateral region presents cavities from a defective cell separation, suggesting that lysis may be indirectly caused by the separation defect (Fig. 10 C).

Sorbitol protects the cells, allowing the activation of a compensatory mechanism that generates a remedial cell wall that extends as a secondary septum at both sides of the twisted primary septum, in a sequential process similar to that of *S. cerevisiae* (Cabib et al., 2001). In some cases, only one sister cell displays primary septum remnants in the new end after side-explosive separation, suggesting a defective primary–secondary septum association and a linking role for α-glucan. Additionally, primary and secondary septum synthesis might need to be coupled in order to generate the required linkages for a compact septum. Similar compensatory mechanisms have been described in Bgs1- and Bgs4-depleted cells and other α(1-3)glucan-containing fungi (Cortés et al., 2005, 2007; Maubon et al., 2006; Reese et al., 2007; Farkas et al., 2009). *S. pombe* contains four additional Ags proteins, which are detected during sporulation (García et al., 2006). Evaluation of the activities induced by this compensatory mechanism will require further genetic and molecular analysis of Ags and Bgs subunits.

Materials and methods

Strains and culture conditions

The *S. pombe* strains used in this study are enumerated in Table S1. *ags1*Δ deletion was performed in a diploid strain by removing the entire coding sequence of an *ags1*$^+$ copy, as described for *bgs1*$^+$, *bgs3*$^+$, and *bgs4*$^+$ gene deletions (Cortés et al., 2002, 2005, 2007). Tetrad analysis of sporulated *ags1*$^+$/*ags1*Δ diploids showed Ags1 to be essential, as described by previous work (Katayama et al., 1999). Haploid *ags1*Δ strains were maintained viable by transforming the heterozygous *ags1*$^+$/*ags1*Δ diploid with *ags1*$^+$-expressing plasmids and selecting haploid spore clones containing the *ags1*Δ deletion, which contained the corresponding *ags1*$^+$ plasmid needed to maintain the cell viable.

*ags1*Δ::*ura4*$^+$ p41XH-*ags1*$^+$ strain 1804 (*his3*$^+$ selection) contains *ags1*$^+$ expressed under the control of the 41X version (medium expression) of the thiamine-repressible *nmt1*$^+$ promoter (Moreno et al., 2000). Other strains with different levels of *ags1*$^+$ repression were made by genetic cross with strain 285 (Leu$^-$, Ura$^-$, His$^-$) transformed with the corresponding version of p81XL-*ags1*$^+$ and p41XL-*ags1*$^+$ (*S. cerevisiae LEU2* selection) and selection of Leu$^+$, Ura$^+$, His$^-$ clones.

81X-*ags1*$^+$ strain 2086 contains the selection marker *ura4*$^+$ adjacent to the *nmt1*$^+$-81X promoter, followed by the *ags1*$^+$ ORF. This strain was made from a diploid strain by homologous recombination of an ApaI–ApaI fragment of pSK-P*ags1*$^+$-*ura4*$^+$-81X-*ags1*$_{1\text{-}2603}$ (see below) and sporulation. The resulting 81X-*ags1*$^+$ haploid strain contained one single integrated *ags1*$^+$ copy under the control of the 81X promoter and exhibited a strong lytic phenotype in the presence of thiamine (repressed conditions) and a wild-type phenotype in its absence (induced conditions).

81X-*ags1*$^+$ 81X-*bgs1*$^+$ strain 4825 was made by a genetic cross between strains 2086 (81X-*ags1*$^+$, Ura$^+$) and 2234 (81X-*bgs1*$^+$, Ura$^-$, 5-fluoroorotic acid [FOA] selection) and random spore selection of Ura$^+$ clones (81X-*ags1*$^+$), followed by the analysis of the possible differential phenotype in the presence of thiamine between single 81X-*ags1*$^+$ and double 81X-*ags1*$^+$ 81X-*bgs1*$^+$ strains. PCR analysis of positive clones confirmed the presence of the 81X promoter and the absence of the original promoter in both genes.

The 11.3 kb *ags1*$^+$-containing fragment seemed to be toxic for cloning. Therefore, the *ags1*Δ strain containing an integrated *ags1*$^+$-*GFP* copy was made sequentially with two overlapping fragments that restore the entire *ags1*$^+$ sequence (Fig. S1 A). First, strain 1804 (*ags1*Δ::*ura4*$^+$ p41XH-*ags1*$^+$, *his3*$^+$ selection) was made Ura$^-$ by transformation with a *ura4*$^+$-empty *ags1*Δ deletion cassette and colony selection in minimal medium containing FOA to make strain 2881 (*ags1*Δ p41XH-*ags1*$^+$). Then, the *ags1*Δ p41XH-*ags1*$^+$ strain was transformed with SpeI-cut pSK-*ura4*$^+$-*ags1*$_{3704\text{-}7233}$ (*ura4*$^+$ selection, 3.5 kb *ags1*$^+$ 3′ORF, and 1.3 kb 3′UTR), which directed its integration at the SpeI site at position +431 of *ags1*$^+$ 3′UTR. Correct integration was confirmed by PCR analysis using pairs of oligonucleotides external and internal to the integrated fragment. The resulting strain 2939 (*ags1*Δ 3′UTR*ags1*$^+$::*ags1*$_{3704\text{-}7233}$:*ura4*$^+$ p41XH-*ags1*$^+$) was transformed with AgeI-cut pJK-*ags1*$_{1\text{-}6267}$-*GFP* (*leu1*$^+$ selection, 2.9 kb promoter, 6.2 kb *ags1*$^+$ 5′ORF, and 0.7 kb *12A-GFP-12A* inserted in frame at base 5866 of *ags1*$^+$ ORF, see below), which directed its integration at the AgeI site at base 6025 in the *ags1*$^+$ 3′ORF, and restored the complete *ags1*$^+$ coding sequence (Fig. S1 A). To eliminate p41XH-*ags1*$^+$, to confirm *ags1*$^+$ reconstruction, and to analyze Ags1-GFP functionality, this strain was crossed with strain 285 (Leu$^-$, Ura$^-$, His$^-$) and tetrad analysis was performed. Leu and Ura phenotypes always co-segregated 2+:2− as expected after *ags1*$^+$ restoration. p41XH-*ags1*$^+$ was lost in most of the clones as a result of the sporulation process. The obtained *ags1*Δ *ags1*$^+$-*GFP* strain displayed a wild-type phenotype under all tested conditions and expressed Ags1-GFP at physiological levels from a single integrated *ags1*$^+$-*GFP* gene under the control of its own promoter. Similarly, an *ags1*Δ *ags1*$^+$-*RFP* strain expressing a fully functional Ags1-RFP (Cherry variant; Shaner et al., 2005) from pJK-*ags1*$_{1\text{-}6267}$-*Cherry* was also made.

Standard complete yeast growth (YES), selective (EMM), and sporulation (SPA) media (Egel, 1984; Alfa et al., 1993) have already been described. Cell growth was monitored by measuring the A_{600} of early log-phase cell cultures in a Coleman Junior II spectrophotometer (OD_{600} 0.15 = 10^7 cells/ml). For serial dilution drop tests of growth, early log-phase cells growing at 25°C were adjusted to 10^7 cells/ml and then serially diluted

Published August 13, 2012

1:10. The different dilutions were spotted onto YES and YES + 1.2 M sorbitol plates, incubated for 2–3 d at the indicated temperatures, and photographed. Latrunculin A (Lat A; Enzo Life Sciences) was used at a 100-µM final concentration (from a stock of 10 mM in DMSO). Methyl benzimidazol-2-yl-carbamate (MBC; Sigma-Aldrich) was used at a 25-µg/ml final concentration (from a stock of 5 mg/ml in DMSO). General procedures for yeast and bacterial culture and genetic manipulations were performed as described previously (Moreno et al., 1991; Sambrook and Russell, 2001).

Plasmids and DNA techniques

pSK-*ags1*$^+$ is an 11.3-kb EcoRI–ApaI DNA fragment containing the *ags1*$^+$ gene sequence cloned in two steps into the Bluescript SK$^+$ vector. First, a 7.9-kb EcoRI–SalI 5′-*ags1*$^+$ fragment (5.1 kb of *ags1*$^+$ ORF) from pDB248X-*ags1*$^+$ (a gift from Takashi Toda, London Research Institute, Cancer Research UK, London, UK), and then a 3.4-kb SalI–ApaI 3′-*ags1*$^+$ fragment (2.1 kb of *ags1*$^+$ ORF) PCR-amplified from genomic DNA, were cloned.

The 7.2-kb *ags1*$^+$ ORF sequence from pSK-*ags1*$^+$ containing the sites NotI before the start codon and BamHI after the termination codon, inserted by site-directed mutagenesis, was cloned into NotI–BamHI of pJR2-81XL, pJR2-41XL, and pJR2-41XH (*S. cerevisiae LEU2* and *S. pombe his3*$^+$ selection, and 81X and 41X versions of the thiamine-repressible *nmt1*$^+$ promoter, respectively; Moreno et al., 2000). The levels of *ags1*$^+$ repression from the resulting 81X and 41X plasmids were analyzed in an *ags1*Δ background. All the strains displayed a lethal lytic phenotype in repressed conditions (presence of thiamine) even with the 41X promoter, and the wild-type phenotype in induced conditions (absence of thiamine). As expected, lysis and cell growth arrest appeared earlier in 81X-*ags1*$^+$ strains due to their reduced *ags1*$^+$ expression. To find the optimal *ags1*$^+$ repression level, three increasing deletions (AscI–NotI, SacII–NotI and NruI–NotI) in the multiple cloning site (MCS) were made to approach *ags1*$^+$ ORF and 81X promoter, thus gradually increasing the *ags1*$^+$ expression level as described for *bgs1*$^+$ (Cortés et al., 2007). The optimal 81X-*ags1*$^+$ repression conditions were achieved with the MCS NruI–NotI deletion between 81X promoter and *ags1*$^+$ ORF. The lysis was only slightly slower but the appearance of revertant survivors observed with the other constructs decreased.

The *ags1*$^+$ shut-off phenotype of strains containing multicopy p81X-*ags1*$^+$ plasmids was heterogeneous and the appearance of revertant or attenuated clones was detected. To obtain a strain with a more uniform and stable *ags1*$^+$ shut-off phenotype that could be useful to study the Ags1 absence effect, a strain with an integrated 81X-*ags1*$^+$ single copy was made (see above). To ensure that the low expression level of a single 81X-*ags1*$^+$ copy would still be able to maintain wild-type cells under induced conditions, the 81X-*ags1*$^+$ MCS-NruI/NotIΔ sequence was selected. pSK-P*ags1*$^+$-*ura4*$^+$-81X-*ags1*$_{1\text{-}2603}$ contains an *ags1*$^+$ promoter fragment (−2125 to −1099), the *ura4*$^+$ sequence, and an 81X-*ags1*$^+$ 5′ORF fragment (+1 to +2603) from p81XL-*ags1*$^+$ MCS-NruI/NotIΔ. An ApaI–ApaI P*ags1*$^+$-*ura4*$^+$-81X-*ags1*$_{1\text{-}2603}$ fragment was used as a substitution cassette to make the integrated 81X-*ags1*$^+$ strains. Similarly, a 41X-*ags1*$^+$ MCS-NruI/NotIΔ strain was made and analyzed as well.

pSK-*ura4*$^+$-*ags1*$_{3704\text{-}7233}$ (*ura4*$^+$ selection) is a 4.8-kb BstBI–ApaI fragment containing 3.5 kb of *ags1*$^+$ 3′ORF and 1.3 kb of *ags1*$^+$ 3′UTR cloned into ClaI–ApaI sites of pSK-*ura4*$^+$ (Moreno et al., 2000). pJK-*ags1*$_{1\text{-}6267}$ is the integrative pJK148 (*leu1*$^+$ selection) with a 9.1-kb ApaI–NheI fragment, containing 2.9 kb of *ags1*$^+$ promoter and 6.2 kb of *ags1*$^+$ 5′ORF, overlapping 2.5 kb of the above *ags1*$^+$ 3′ORF fragment (Fig. S1 A). Cut-directed integration and recombination between both plasmids restored the complete *ags1*$^+$ coding sequence (see above strains).

To provide a flexible linker between GFP and the target proteins, a 12-alanine coding sequence was fused to the *GFP* 5′ and/or 3′-end of pKS-*GFP* (Cortés et al., 2002), making pKS-*GFP-12A*, pKS-*12A-GFP*, and pKS-*12A*-GFP-12A*. *12A** indicates a nucleotide sequence different from *12A*, thus avoiding homologous recombination.

To obtain a functional GFP-fused Ags1 and because bioinformatic algorithms predicted a putative signal peptide in the Ags1 N terminus, an Ags1 C-terminal GFP tagging was analyzed first. An *ags1*Δ strain containing *ags1-GFP* 3′ORF from pSK-*ura4*$^+$-*ags1*$_{3704\text{-}7233}$-*GFP* (*ura4*$^+$ selection, 3.5 kb *ags1*$^+$ 3′ORF, 1.3 kb 3′UTR, and *12A-GFP* inserted in frame before the TAG stop codon) integrated into the *ags1*$^+$ 3′UTR (see above) was transformed with overlapping AgeI-cut pJK-*ags1*$_{1\text{-}6267}$ (*leu1*$^+$ selection, 2.9 kb promoter, 6.2 kb *ags1*$^+$ 5′ORF), restoring the complete *ags1*$^+$-*GFP* coding sequence (see above). However, the resulting Ags1-GFP fusion was nonfunctional in an *ags1*Δ background. Similarly, an *ags1*Δ strain containing *ags1* 3′ORF from pSK-*ura4*$^+$-*ags1*$_{3704\text{-}7233}$ was transformed with AgeI-cut pJK-*GFP-ags1*$_{1\text{-}6267}$ (*GFP-12A* inserted in frame after the ATG start codon), but the resulting N-terminal GFP-Ags1 fusion was also nonfunctional (Fig. 1 A).

Due to the possibility of a signal peptide, GFP inserted at different sites just before or after the predicted cleavage site of Ags1 (aa 26–27) was analyzed. The *12A*-GFP-12A* sequence was inserted in-frame at *ags1*$^+$ bases 73, 82, 85, 91, 97, and 103 (aa 25, 28, 29, 31, 33, and 35, respectively) of pJK-*ags1*$_{1\text{-}6267}$. As before, the resulting GFP-Ags1 fusions were nonfunctional (Fig. 1 A).

Next, the five most hydrophilic regions of both α-amylase and glycogen synthase domains of Ags1 (Hochstenbach et al., 1998), as deduced from hydropathy analysis, were selected. A hydropathy plot was generated using Membrane Protein Explorer software (MPEx, ver. 3.2; Snider et al., 2009) with an octanol Wimley-White scale and a window size of 19. The amino acids predicted at the boundaries between secondary structures were then chosen, as described for Bgs4 (Cortés et al., 2005). As a result, the *12A*-GFP-12A* sequence was inserted in-frame at *ags1*$^+$ bases 229, 3178, 3265, 3298, and 5866 (aa 77, 1060, 1089, 1100, and 1956, respectively) of pJK-*ags1*$_{1\text{-}6267}$. Only pJK-*ags1*$_{1\text{-}6267}$-*GFP* with *12A*-GFP-12A* inserted at base 5866 (aa 1956) created a functional Ags1-GFP in an *ags1*Δ background (strain 3166, see above and Table S1), and therefore, it was selected for Ags1 localization studies at the physiological level (Fig. 1 A).

The Cherry variant of the monomeric mRFP1 protein (Shaner et al., 2005) was used to create a functional Ags1-RFP fusion. pKS-*Cherry* is pKS$^+$ with a BamHI–EcoRI fragment containing the 678-bp *Cherry* ORF from pRSET-*Cherry* (provided by R.Y. Tsien, University of California, San Diego, La Jolla, CA). pKS-*8A-Cherry-12A* is pKS-*Cherry* with 8- and 12-alanine coding sequences fused to *Cherry* 5′ and 3′-end, respectively. pJK-*ags1*$_{1\text{-}6267}$-*Cherry* is pJK-*ags1*$_{1\text{-}6267}$ with *8A-Cherry-12A* inserted at base 5866 (amino acid 1956). The *ags1*Δ *ags1*$^+$*-RFP* strain (Table S1) expressed a functional Ags1-RFP and therefore, it was selected for Ags1 localization studies at the physiological level.

Immunoprecipitation and immunoblot analysis

10^9 early log-phase cells expressing the different tagged proteins were harvested, washed with stop solution (154 mM NaCl, 10 mM EDTA, 10 mM NaN_3, and 10 mM NaF), then with buffer (50 mM Tris-HCl, pH 7.5, 5 mM EDTA) suspended in lysis buffer (50 mM Tris-HCl pH 7.5, 5 mM EDTA, 200 mM NaCl containing 100 µM phenylmethylsulphonylfluoride and 2 µg/ml leupeptin and aprotinin) and broken with glass beads (FastPrep FP120, 3 × 15 s, speed of 5.5 [BIO 101; Savant]). Cell walls were removed by centrifugation (4,500 *g*, 1 min, 4°C). The supernatant was collected and cell membranes were pelleted by centrifugation (16,000 *g*, 1 h, 4°C), suspended in 200 µl of immunoprecipitation buffer (IPB; 50 mM Tris-HCl, pH 7.5, 5 mM EDTA, 200 mM NaCl, 0.5% Tween 20, 100 µM phenylmethylsulphonylfluoride, and 2 µg/ml leupeptin and aprotinin), and agitated (1,300 rpm, 15 min, 1°C; Thermomixer Comfort, Eppendorf). Next, the membrane suspension was centrifuged (21,000 *g*, 30 min, 4°C); the supernatant was collected, diluted with IPB, and the solubilized membrane proteins were incubated with protein G–Sepharose 4 Fast Flow beads (GE Healthcare) coated with anti-GFP serum (Molecular Probes, Invitrogen) for 4 h at 4°C. The beads were washed three times with IPB and suspended in sample buffer.

Proteins were separated by 3–8% Tris-Acetate SDS–PAGE (NuPAGE; Invitrogen), transferred to Immobilon-P membranes (EMD Millipore), and blotted to detect the GFP- or HA-fused epitopes with the corresponding antibodies (monoclonal JL-8 anti-GFP 1:500 [Living colors; Takara Bio Inc.]; and monoclonal anti-HA 1:10,000 [Roche]), and the enhanced chemiluminescence (ECL) detection kit (GE Healthcare). Western blot analysis of solubilized membrane proteins (40 µg of total protein) was performed to determine the total amount of tagged protein.

Labeling and fractionation of cell wall polysaccharides

[^{14}C]glucose labeling and fractionation of cell wall polysaccharides were performed essentially as described previously (Ishiguro et al., 1997). Exponentially growing cells incubated at 28°C in EMM or EMM + 1.2 M sorbitol were diluted with the same medium, supplemented with D-[U-^{14}C]glucose, as specified for each case of *ags1*$^+$ shut-off (10 µCi/ml for short labeling in EMM and 5 µCi/ml for longer labeling in EMM + 1.2 M sorbitol), and they were collected at the indicated times. Total glucose incorporation was monitored by measuring radioactivity in trichloroacetic acid–insoluble material. Cells were harvested at early logarithmic phase, supplemented with unlabeled cells as the carrier, washed twice with 1 mM EDTA, and broken with glass beads in a FastPrep FP120 apparatus (3 × 20 s, speed of 6.0 [BIO 101; Savant]). Cell walls were purified by repeated washing and differential centrifugation (once with 1 mM EDTA, twice with 5 M NaCl, and twice with 1 mM EDTA) at 1,000 *g* for 5 min. Finally, purified cell walls were heated at 100°C for 5 min. Cell wall samples were extracted with 6% NaOH for 60 min at 80°C and neutralized with acetic acid.

Published August 13, 2012

Precipitation of the galactomannan fraction from the neutralized supernatant was performed with Fehling reagent by adding unlabeled yeast mannan as the carrier, as described previously (Algranati et al., 1966). Other samples of cell wall suspension were incubated with Zymolyase 100T (250 µg of enzyme and 1/10 volume of cell wall suspension; AMS Biotechnology) in 50 mM citrate-phosphate buffer (pH 5.6) for 24 h at 30°C. Samples without enzyme were included as a control. After incubation, samples were centrifuged and washed with the same buffer. 1 ml of 10% trichloroacetic acid was added to the pellets, filtered in Whatman GF/C glass fiber filters (3 × 1 ml of 10% trichloroacetic acid and 2 × 1 ml of ethanol), and their radioactivity levels were measured in a scintillation counter (Beckman Coulter). These pellets were considered the α-glucan fraction, and supernatants were the β-glucan-plus-galactomannan fraction. β-Glucan was calculated as radioactivity remaining after subtraction of galactomannan and α-glucan from total cell wall incorporation. All determinations were performed in duplicate, and data for each strain were calculated from three independent cultures.

Microscopy techniques

For Calcofluor white fluorescence, early logarithmic-phase cells were visualized directly by adding a solution of Calcofluor white (CW; 50 µg/ml final concentration) to the sample and using the appropriate UV filter. Images were obtained with a fluorescence microscope (model DM RXA; Leica), a PL APO 63×/1.32 oil PH3 objective, a digital camera (model DFC350FX; Leica) and CW4000 cytoFISH software (Leica). Images were processed with Adobe Photoshop software. For time-lapse imaging, 0.3–0.6 ml of log-phase cells were collected by low speed centrifugation (3,000 *g* for 1 min), suspended in 0.3 ml of EMM or EMM + 1.2 M sorbitol (with 20 µg/ml thiamine for cells repressing *ags1*$^+$) containing CW (5 µg/ml final concentration) when necessary, and placed in a well from a µ-Slide 8 well (80821-Uncoated; Ibidi) previously coated with 10 µl of 1 mg/ml soybean lectin (L1395; Sigma-Aldrich). Time-lapse experiments were made at 28°C or the specified temperature by acquiring epifluorescence and/or phase-contrast cell images in single planes and 1 × 1 binning on an inverted microscope (model IX71; Olympus) equipped with a PlanApo 100x/1.40 IX70 objective and a Personal DeltaVision system (Applied Precision). Images were captured using a CoolSnap HQ2 monochrome camera (Photometrics) and softWoRx 5.5.0 release 6 imaging software (Applied Precision). Subsequently, GFP and RFP time-lapse images were restored and corrected by 3D Deconvolution (conservative ratio, 10 iterations and medium noise filtering) through softWoRx imaging software. Next, images were processed with ImageJ (National Institutes of Health, Bethesda, MD) and Adobe Photoshop software.

For FITC-conjugated concanavalin A staining, equal amounts of log-phase *hht1*$^+$*-RFP* (control wild type, nucleus labeling) and 81X-*ags1*$^+$ cells were mixed, washed with PBS (3,000 *g* for 1 min), suspended in 0.5 ml PBS containing 100 µg/ml FITC-conjugated concanavalin A (C7642; Sigma-Aldrich), and incubated at 28°C for 20 min in the dark. After incubation, the cells were washed three times with PBS (3,000 *g* for 1 min), resuspended in 10 µl PBS, and visualized for FITC and RFP fluorescence. Fluorescence intensity analysis of FITC-conjugated concanavalin A staining was made with ImageJ software by placing a fixed square on the cell poles and measuring maximal fluorescence.

Transmission electron microscopy

Early log-phase cells were fixed with 2% glutaraldehyde EM (GA; Electron Microscopy Science) in 50 mM phosphate buffer, pH 7.2, and 150 mM NaCl (PBS) for 2 h at 4°C, post-fixed with 1.2% potassium permanganate overnight at 4°C, and embedded in Quetol 812 as described previously (Konomi et al., 2003). Ultrathin sections were stained in 4% uranyl acetate and 0.4% lead citrate, and viewed with a transmission electron microscope (model H-800; Hitachi) operating at 125 kV.

Scanning electron microscopy

Early log-phase cells were placed in a slide coated with 5 mg/ml soybean lectin (L1395; Sigma-Aldrich), prefixed overnight with 2.5% glutaraldehyde at 4°C, washed three times with 100 mM phosphate buffer, pH 7.4, and post-fixed with 1% osmium tetroxide (OsO4) at 4°C for 1 h. Next, the cells were washed three times with water, dehydrated in graded acetone series (30, 50, and 70% for 10 min; 90% for 20 min; and 100% twice for 20 and 30 min), critical-point dried, coated with gold, and visualized with a scanning electron microscope (model DSM 940; Carl Zeiss) operating at 30 kV.

Online supplemental material

Fig. S1 shows a scheme of the steps followed to obtain a fully functional *ags1*$^+$*-GFP* strain and images of Ags1 localization during the cell cycle and sexual differentiation and of Ags1–Bgs1 colocalization. Fig. S2 shows time-lapse images of Ags1 localization in different SIN mutants, showing that Ags1 does not depend on the SIN pathway for its movement from the poles to the medial zone during cytokinesis. Fig. S3 shows genetic interactions of *ags1*$^+$ with *bgs1*$^+$ and SIN genes. The loss of Bgs1 or SIN function suppresses the lytic phenotype of Ags1 absence or *mok1-664* mutation. Fig. S4 shows images of the immediate side-explosive cell separation in the absence of Ags1 or in the *mok1-664* mutant showing the CW-stained primary septum remnants in the new pole of both or just one sister cell. Video 1 shows time-lapse of a representative field of lysis in either one or both sister cells at the beginning of cell separation of Ags1-depleted cells. Videos 2 and 5 show time-lapses of a representative field (2) or a single cell (5) of the progressive and symmetrical cell separation of wild-type cells. Videos 3, 4, and 6–9 show time-lapses of representative fields (3, 4) or single cells (6–9) of the instantaneous and asymmetrical cell separation of Ags1-depleted cells, either without (3, 6, and 7) or with sorbitol (4, 8, and 9). Video 10 shows time-lapse of Ags1-depleted sister cells remaining attached by their side-contact region for at least two cell cycles. Table S1 lists the fission yeast strains used in this study. Online supplemental material is available at http://www.jcb.org/cgi/content/full/jcb.201202015/DC1.

This paper is dedicated to Professor Enrico Cabib, who taught us to vouch for the small and defenseless yeasts, on the occasion of his retirement and his outstanding contributions in the field of yeast cell wall and morphogenesis. We thank E. Cabib for comments on the manuscript; Emma Keck for language revision; Carlos Sacristán for technical help with the drop tests; T. Toda for *ags1*$^+$-containing plasmid; R.Y. Tsien for RFP-containing plasmids; and P. Munz, P. Nurse, F. Chang, V. Simanis, M. H. Valdivieso, and P. Pérez for strains.

We thank the Ramón Areces Foundation for IBFG financial support. J.C.G. Cortés acknowledges support from "Juan de la Cierva" program granted by Minsterio de Ciencia e Innovación (MICINN, Spain). This work was supported by grants BIO2009-10597 (MICINN) and CSI038A11-2 (Junta de Castilla y León, Spain).

Submitted: 2 February 2012
Accepted: 13 July 2012

References

Alfa, C., P. Fantes, J. Hyams, M. McLeod, and E. Warbrick. 1993. Experiments with fission yeast: A laboratory course manual. Cold Spring Harbor Laboratory Press, Cold Spring Harbor, NY.

Algranati, I.D., N. Behrens, H. Carminatti, and E. Cabib. 1966. Mannan synthetase from yeast. *In* Methods Enzymol. Vol. 8. Academic Press. 411–416.

Balasubramanian, M.K., B.R. Hirani, J.D. Burke, and K.L. Gould. 1994. The *Schizosaccharomyces pombe cdc3*$^+$ gene encodes a profilin essential for cytokinesis. *J. Cell Biol.* 125:1289–1301. http://dx.doi.org/10.1083/jcb.125.6.1289

Barral, Y., and D. Liakopoulos. 2009. Role of spindle asymmetry in cellular dynamics. *Int Rev Cell Mol Biol.* 278:149–213. http://dx.doi.org/10.1016/S1937-6448(09)78004-9

Bathe, M., and F. Chang. 2010. Cytokinesis and the contractile ring in fission yeast: towards a systems-level understanding. *Trends Microbiol.* 18:38–45. http://dx.doi.org/10.1016/j.tim.2009.10.002

Cabib, E., D.H. Roh, M. Schmidt, L.B. Crotti, and A. Varma. 2001. The yeast cell wall and septum as paradigms of cell growth and morphogenesis. *J. Biol. Chem.* 276:19679–19682. http://dx.doi.org/10.1074/jbc.R000031200

Chang, F., A. Woollard, and P. Nurse. 1996. Isolation and characterization of fission yeast mutants defective in the assembly and placement of the contractile actin ring. *J. Cell Sci.* 109:131–142.

Cortés, J.C.G., J. Ishiguro, A. Durán, and J.C. Ribas. 2002. Localization of the (1,3)β-D-glucan synthase catalytic subunit homologue Bgs1p/Cps1p from fission yeast suggests that it is involved in septation, polarized growth, mating, spore wall formation and spore germination. *J. Cell Sci.* 115:4081–4096. http://dx.doi.org/10.1242/jcs.00085

Cortés, J.C.G., E. Carnero, J. Ishiguro, Y. Sánchez, A. Durán, and J.C. Ribas. 2005. The novel fission yeast (1,3)β-D-glucan synthase catalytic subunit Bgs4p is essential during both cytokinesis and polarized growth. *J. Cell Sci.* 118:157–174. http://dx.doi.org/10.1242/jcs.01585

Cortés, J.C.G., M. Konomi, I.M. Martins, J. Muñoz, M.B. Moreno, M. Osumi, A. Durán, and J.C. Ribas. 2007. The (1,3)β-D-glucan synthase subunit Bgs1p is responsible for the fission yeast primary septum formation. *Mol. Microbiol.* 65:201–217. http://dx.doi.org/10.1111/j.1365-2958.2007.05784.x

Edwards, J.A., E.A. Alore, and C.A. Rappleye. 2011. The yeast-phase virulence requirement for α-glucan synthase differs among *Histoplasma capsulatum* chemotypes. *Eukaryot. Cell*. 10:87–97. http://dx.doi.org/10.1128/EC.00214-10

Egel, R. 1984. Two tightly linked silent cassettes in the mating-type region of *Schizosaccharomyces pombe. Curr. Genet.* 8:199–203. http://dx.doi.org/10.1007/BF00417816

Fankhauser, C., A. Reymond, L. Cerutti, S. Utzig, K. Hofmann, and V. Simanis. 1995. The *S. pombe cdc15* gene is a key element in the reorganization of F-actin at mitosis. *Cell*. 82:435–444. http://dx.doi.org/10.1016/0092-8674(95)90432-8

Farkas, V., K. Takeo, D. Maceková, M. Ohkusu, S. Yoshida, and M. Sipiczki. 2009. Secondary cell wall formation in *Cryptococcus neoformans* as a rescue mechanism against acid-induced autolysis. *FEM. Yeast Res.* 9:311–320. http://dx.doi.org/10.1111/j.1567-1364.2008.00478.x

Feierbach, B., and F. Chang. 2001. Roles of the fission yeast formin for3p in cell polarity, actin cable formation and symmetric cell division. *Curr. Biol.* 11:1656–1665. http://dx.doi.org/10.1016/S0960-9822(01)00525-5

García, I., V. Tajadura, V. Martín, T. Toda, and Y. Sánchez. 2006. Synthesis of α-glucans in fission yeast spores is carried out by three α-glucan synthase paralogues, Mok12p, Mok13p and Mok14p. *Mol. Microbiol.* 59:836–853. http://dx.doi.org/10.1111/j.1365-2958.2005.04995.x

Goldstein, I.J. 2002. Lectin structure-activity: the story is never over. *J. Agric. Food Chem.* 50:6583–6585. http://dx.doi.org/10.1021/jf0201879

Grün, C.H., F. Hochstenbach, B.M. Humbel, A.J. Verkleij, J.H. Sietsma, F.M. Klis, J.P. Kamerling, and J.F. Vliegenthart. 2005. The structure of cell wall α-glucan from fission yeast. *Glycobiology*. 15:245–257. http://dx.doi.org/10.1093/glycob/cwi002

Hachet, O., and V. Simanis. 2008. Mid1p/anillin and the septation initiation network orchestrate contractile ring assembly for cytokinesis. *Genes Dev.* 22:3205–3216. http://dx.doi.org/10.1101/gad.1697208

Harris, S.D. 2011. Hyphal morphogenesis: an evolutionary perspective. *Fungal Biol*. 115:475–484. http://dx.doi.org/10.1016/j.funbio.2011.02.002

Hartland, R.P., C.A. Vermeulen, F.M. Klis, J.H. Sietsma, and J.G. Wessels. 1994. The linkage of (1-3)-β-glucan to chitin during cell wall assembly in *Saccharomyces cerevisiae. Yeast*. 10:1591–1599. http://dx.doi.org/10.1002/yea.320101208

Henry, C., J.P. Latgé, and A. Beauvais. 2012. α1,3 glucans are dispensable in Aspergillus fumigatus. *Eukaryot. Cell*. 11:26–29. http://dx.doi.org/10.1128/EC.05270-11

Hochstenbach, F., F.M. Klis, H. van den Ende, E. van Donselaar, P.J. Peters, and R.D. Klausner. 1998. Identification of a putative α-glucan synthase essential for cell wall construction and morphogenesis in fission yeast. *Proc. Natl. Acad. Sci. USA*. 95:9161–9166. http://dx.doi.org/10.1073/pnas.95.16.9161

Horisberger, M., and M. Rouvet-Vauthey. 1985. Cell wall architecture of the fisson yeast *Schizosaccharomyces pombe. Experientia*. 41:748–750. http://dx.doi.org/10.1007/BF02012578

Humbel, B.M., M. Konomi, T. Takagi, N. Kamasawa, S.A. Ishijima, and M. Osumi. 2001. In situ localization of β-glucans in the cell wall of *Schizosaccharomyces pombe. Yeast*. 18:433–444. http://dx.doi.org/10.1002/yea.694

Ishiguro, J., and W. Kobayashi. 1996. An actin point-mutation neighboring the 'hydrophobic plug' causes defects in the maintenance of cell polarity and septum organization in the fission yeast *Schizosaccharomyces pombe*. *FEBS Lett.* 392:237–241. http://dx.doi.org/10.1016/0014-5793(96)00819-8

Ishiguro, J., A. Saitou, A. Durán, and J.C. Ribas. 1997. *cps1*$^{+}$, a *Schizosaccharomyces pombe* gene homolog of *Saccharomyces cerevisiae FKS* genes whose mutation confers hypersensitivity to cyclosporin A and papulacandin B. *J. Bacteriol.* 179:7653–7662.

Iwai, H., N. Masaoka, T. Ishii, and S. Satoh. 2002. A pectin glucuronyltransferase gene is essential for intercellular attachment in the plant meristem. *Proc. Natl. Acad. Sci. USA*. 99:16319–16324. http://dx.doi.org/10.1073/pnas.252530499

Johnson, B.F., B.Y. Yoo, and G.B. Calleja. 1973. Cell division in yeasts: movement of organelles associated with cell plate growth of *Schizosaccharomyces pombe. J. Bacteriol.* 115:358–366.

Katayama, S., D. Hirata, M. Arellano, P. Pérez, and T. Toda. 1999. Fission yeast α-glucan synthase Mok1 requires the actin cytoskeleton to localize the sites of growth and plays an essential role in cell morphogenesis downstream of protein kinase C function. *J. Cell Biol.* 144:1173–1186. http://dx.doi.org/10.1083/jcb.144.6.1173

Konomi, M., K. Fujimoto, T. Toda, and M. Osumi. 2003. Characterization and behaviour of α-glucan synthase in *Schizosaccharomyces pombe* as revealed by electron microscopy. *Yeast*. 20:427–438. http://dx.doi.org/10.1002/yea.974

Krapp, A., and V. Simanis. 2008. An overview of the fission yeast septation initiation network (SIN). *Biochem. Soc. Trans.* 36:411–415. http://dx.doi.org/10.1042/BST0360411

Krapp, A., S. Schmidt, E. Cano, and V. Simanis. 2001. *S. pombe* cdc11p, together with sid4p, provides an anchor for septation initiation network proteins on the spindle pole body. *Curr. Biol.* 11:1559–1568. http://dx.doi.org/10.1016/S0960-9822(01)00478-X

Latgé, J.P. 2007. The cell wall: a carbohydrate armour for the fungal cell. *Mol. Microbiol.* 66:279–290. http://dx.doi.org/10.1111/j.1365-2958.2007.05872.x

Liu, J., X. Tang, H. Wang, S. Oliferenko, and M.K. Balasubramanian. 2002. The localization of the integral membrane protein Cps1p to the cell division site is dependent on the actomyosin ring and the septation-inducing network in *Schizosaccharomyces pombe. Mol. Biol. Cell*. 13:989–1000. http://dx.doi.org/10.1091/mbc.01-12-0581

Martín, V., B. García, E. Carnero, A. Durán, and Y. Sánchez. 2003. Bgs3p, a putative 1,3-β-glucan synthase subunit, is required for cell wall assembly in *Schizosaccharomyces pombe. Eukaryot. Cell*. 2:159–169. http://dx.doi.org/10.1128/EC.2.1.159-169.2003

Martins, I.M., J.C.G. Cortés, J. Muñoz, M.B. Moreno, M. Ramos, J.A. Clemente-Ramos, A. Durán, and J.C. Ribas. 2011. Differential activities of three families of specific β(1,3)glucan synthase inhibitors in wild-type and resistant strains of fission yeast. *J. Biol. Chem.* 286:3484–3496. http://dx.doi.org/10.1074/jbc.M110.174300

Maubon, D., S. Park, M. Tanguy, M. Huerre, C. Schmitt, M.C. Prévost, D.S. Perlin, J.P. Latgé, and A. Beauvais. 2006. *AGS3*, an α(1-3) glucan synthase gene family member of *Aspergillus fumigatus*, modulates mycelium growth in the lung of experimentally infected mice. *Fungal Genet. Biol.* 43:366–375. http://dx.doi.org/10.1016/j.fgb.2006.01.006

Moreno, S., A. Klar, and P. Nurse. 1991. Molecular genetic analysis of fission yeast *Schizosaccharomyces pombe. Methods Enzymol.* 194:795–823. http://dx.doi.org/10.1016/0076-6879(91)94059-L

Moreno, M.B., A. Durán, and J.C. Ribas. 2000. A family of multifunctional thiamine-repressible expression vectors for fission yeast. *Yeast*. 16:861–872. http://dx.doi.org/10.1002/1097-0061(20000630)16:9<861::AID-YEA577>3.0.CO;2-9

Osumi, M., N. Yamada, H. Kobori, A. Taki, N. Naito, M. Baba, and T. Nagatani. 1989. Cell wall formation in regenerating protoplasts of *Schizosaccharomyces pombe*: study by high resolution, low voltage scanning electron microscopy. *J. Electron Microsc. (Tokyo)*. 38:457–468.

Pérez, P., and J.C. Ribas. 2004. Cell wall analysis. *Methods*. 33:245–251. http://dx.doi.org/10.1016/j.ymeth.2003.11.020

Pollard, T.D., and J.Q. Wu. 2010. Understanding cytokinesis: lessons from fission yeast. *Nat. Rev. Mol. Cell Biol.* 11:149–155. http://dx.doi.org/10.1038/nrm2834

Reese, A.J., A. Yoneda, J.A. Breger, A. Beauvais, H. Liu, C.L. Griffith, I. Bose, M.J. Kim, C. Skau, S. Yang, et al. 2007. Loss of cell wall α(1-3) glucan affects *Cryptococcus neoformans* from ultrastructure to virulence. *Mol. Microbiol.* 63:1385–1398. http://dx.doi.org/10.1111/j.1365-2958.2006.05551.x

Ribas, J.C., M. Díaz, A. Durán, and P. Pérez. 1991. Isolation and characterization of *Schizosaccharomyces pombe* mutants defective in cell wall (1-3)β-D-glucan. *J. Bacteriol.* 173:3456–3462.

Roberts, J.A., and Z. Gonzalez-Carranza. 2007. Plant cell separation and adhesion. Annual Plant Reviews, Volume 25. Blackwell, Oxford. xii, 210 pp.

Rosenberg, J.A., G.C. Tomlin, W.H. McDonald, B.E. Snydsman, E.G. Muller, J.R. Yates III, and K.L. Gould. 2006. Ppc89 links multiple proteins, including the septation initiation network, to the core of the fission yeast spindle-pole body. *Mol. Biol. Cell*. 17:3793–3805. http://dx.doi.org/10.1091/mbc.E06-01-0039

Sambrook, J., and D.W. Russell. 2001. Molecular cloning: A laboratory manual. Cold Spring Harbor Laboratory Press, Cold Spring Harbor, NY.

Schmidt, M., B. Bowers, A. Varma, D.H. Roh, and E. Cabib. 2002. In budding yeast, contraction of the actomyosin ring and formation of the primary septum at cytokinesis depend on each other. *J. Cell Sci.* 115:293–302.

Shaner, N.C., P.A. Steinbach, and R.Y. Tsien. 2005. A guide to choosing fluorescent proteins. *Nat. Methods*. 2:905–909. http://dx.doi.org/10.1038/nmeth819

Shaw, J.A., P.C. Mol, B. Bowers, S.J. Silverman, M.H. Valdivieso, A. Durán, and E. Cabib. 1991. The function of chitin synthases 2 and 3 in the *Saccharomyces cerevisiae* cell cycle. *J. Cell Biol.* 114:111–123. http://dx.doi.org/10.1083/jcb.114.1.111

Sipiczki, M. 2007. Splitting of the fission yeast septum. *FEM. Yeast Res.* 7:761–770. http://dx.doi.org/10.1111/j.1567-1364.2007.00266.x

Snider, C., S. Jayasinghe, K. Hristova, and S.H. White. 2009. MPEx: a tool for exploring membrane proteins. *Protein Sci.* 18:2624–2628. http://dx.doi.org/10.1002/pro.256

Sparks, C.A., M. Morphew, and D. McCollum. 1999. Sid2p, a spindle pole body kinase that regulates the onset of cytokinesis. *J. Cell Biol.* 146:777–790. http://dx.doi.org/10.1083/jcb.146.4.777

Sugawara, T., M. Sato, T. Takagi, T. Kamasaki, N. Ohno, and M. Osumi. 2003. In situ localization of cell wall α-1,3-glucan in the fission yeast *Schizosaccharomyces pombe. J. Electron Microsc. (Tokyo).* 52:237–242. http://dx.doi.org/10.1093/jmicro/52.2.237

Verde, F., J. Mata, and P. Nurse. 1995. Fission yeast cell morphogenesis: identification of new genes and analysis of their role during the cell cycle. *J. Cell Biol.* 131:1529–1538. http://dx.doi.org/10.1083/jcb.131.6.1529

Verma, D.P., and Z. Hong. 2001. Plant callose synthase complexes. *Plant Mol. Biol.* 47:693–701. http://dx.doi.org/10.1023/A:1013679111111

Wang, H., X. Tang, J. Liu, S. Trautmann, D. Balasundaram, D. McCollum, and M.K. Balasubramanian. 2002. The multiprotein exocyst complex is essential for cell separation in *Schizosaccharomyces pombe. Mol. Biol. Cell.* 13:515–529. http://dx.doi.org/10.1091/mbc.01-11-0542

Win, T.Z., Y. Gachet, D.P. Mulvihill, K.M. May, and J.S. Hyams. 2001. Two type V myosins with non-overlapping functions in the fission yeast *Schizosaccharomyces pombe*: Myo52 is concerned with growth polarity and cytokinesis, Myo51 is a component of the cytokinetic actin ring. *J. Cell Sci.* 114:69–79.

Cortés et al., http://www.jcb.org/cgi/content/full/jcb.201202015/DC1

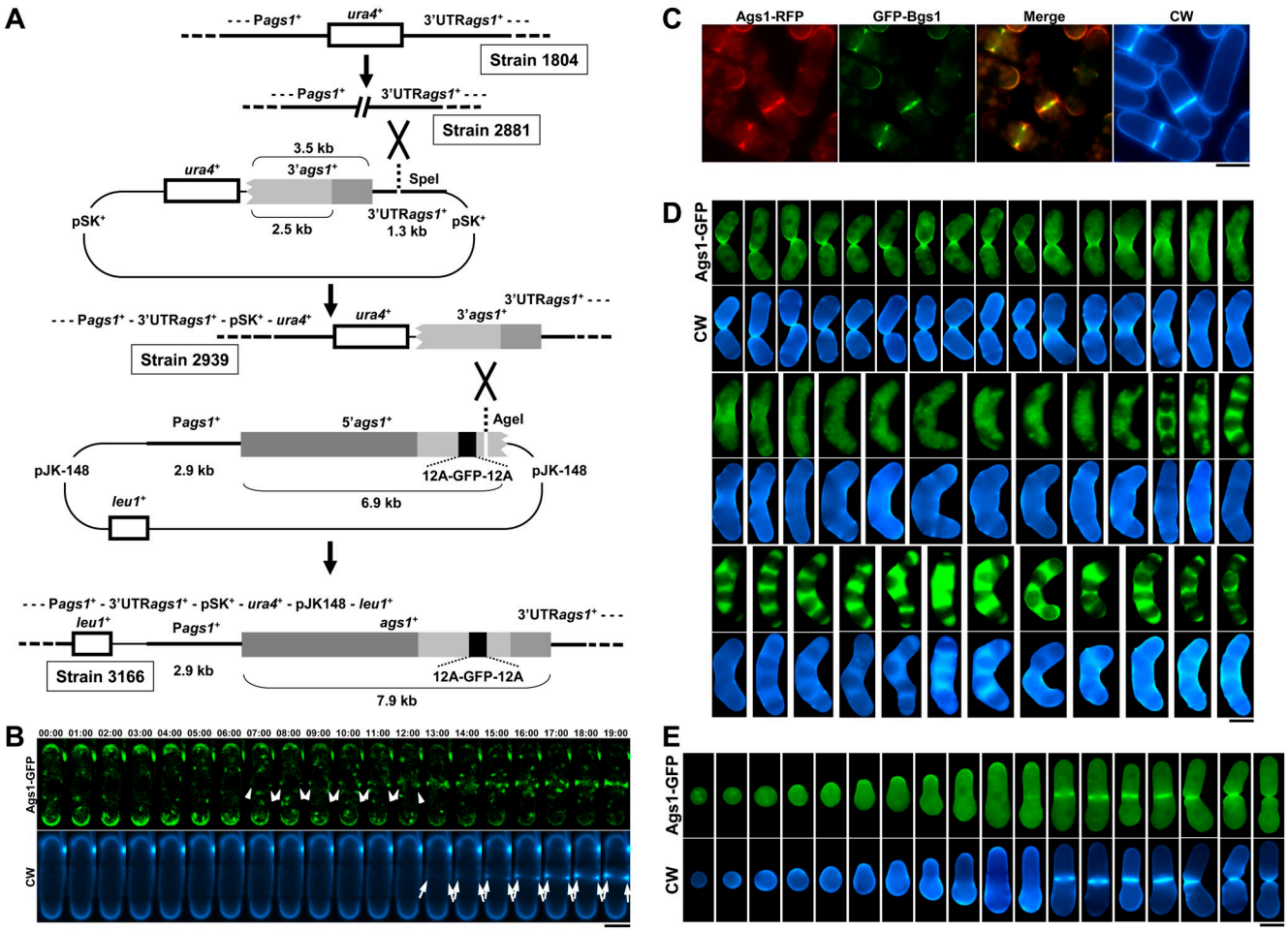

Figure S1. **Like Bgs1, Ags1 localizes to all sites of wall synthesis during both the vegetative and sexual phases of the life cycle.** (A) Scheme showing the sequential steps followed to obtain *ags1*Δ strains containing an integrated *ags1*$^+$*-GFP* copy (see Materials and methods). The *ags1*$^+$ *5′* and 3′ fragments are shown as gray boxes, in which the 2.5-kb overlapping region is shown as a light gray box. The 0.7-kb 12A-*GFP*-12A fragment, shown as a black box, can be inserted into any site of *ags1*$^+$ *5′* sequence, before the AgeI linearization site. (B) Ags1 localizes like Bgs1 in the contractile ring very early in cytokinesis, before the septum is detected by Calcofluor white (CW) staining. However, contrary to Bgs1, Ags1 does not disappear from the poles during cytokinesis until late septation. *ags1*$^+$*-GFP* cells growing in YES medium at 28°C were transferred to fresh YES medium containing 5 µg/ml CW and visualized by time-lapse CW staining and GFP fluorescence microscopy at 28°C. Arrowhead: localization of Ags1 in the medial ring before septum synthesis; Arrow: appearance of the septum structure. Elapsed time is shown in minutes. (C) Ags1 and Bgs1 colocalize at the division site (contractile ring and septum) and growing poles. Early log-phase *ags1*$^+$*-RFP GFP-bgs1*$^+$ cells growing in YES medium at 28°C were visualized for CW staining (50 µg/ml) and GFP and RFP fluorescence. Bar, 5 µm. (D) Ags1 is present and localized to all sites of cell wall synthesis during sexual differentiation. Homothallic *ags1*$^+$*-GFP* h90 cells grown in EMM to early stationary phase were transferred onto SPA plates and incubated at 28°C. Samples were collected after 3, 5, 8, 24, and 48 h and visualized by phase contrast (not depicted), CW staining (50 µg/ml), and GFP fluorescence. Cells and zygotes representative of each mating and sporulation step were selected and ordered to show a sexual phase progression. (E) Ags1 is present and localized to all sites of cell wall synthesis during spore germination. Homothallic *ags1*$^+$*-GFP* h90 strain was grown and sporulated for 10 d as in D. The spores were collected and incubated in YES liquid medium at 28°C. Samples were taken after 2, 3, 7, 8, 9, 10, and 11 h, and observed as in D. Spores illustrative of each germination step were selected and ordered to show a germination progression. Bar, 5 µm.

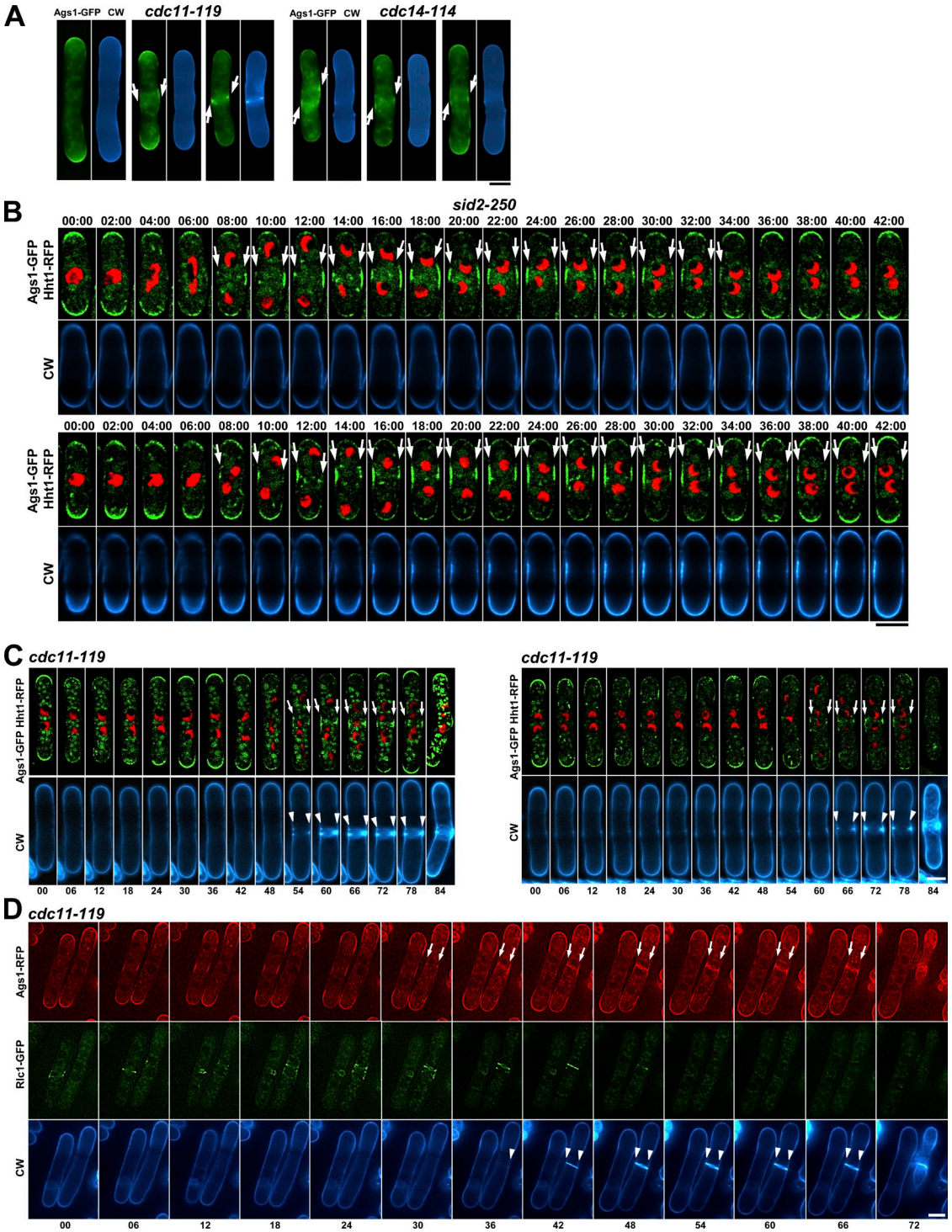

Figure S2. **Ags1 does not depend of the SIN pathway for its movement from the poles to the medial zone during cytokinesis.** (A) SIN mutant cells expressing *ags1⁺-GFP* were grown in YES medium at 25°C and shifted to 36°C for 4 h. (B) *sid2-250 ags1⁺-GFP hht1⁺-RFP* cells growing in YES medium at 25°C were shifted to 36°C for 2 h, transferred to fresh YES medium containing 5 µg/ml CW, and visualized by time-lapse CW staining (5 µg/ml) and GFP and RFP fluorescence at 36°C. Arrow: Ags1-GFP localization in the medial region after nuclear mitosis in the SIN mutant cell. Two examples representative of Ags1-GFP movement from the poles to the medial region after nuclear mitosis (see histone Hht1-RFP) are shown. (C) Ags1 localizes to the medial septum-like structures formed in the absence of a functional SIN. *cdc11-119 ags1⁺-GFP hht1⁺-RFP* cells were grown and visualized as in B. Two examples representative of Ags1-GFP movement and localization to the septum-like structures (see CW staining) after nuclear mitosis (see histone Hht1-RFP) are shown. (D) *cdc11-119 ags1⁺-RFP rlc1⁺-GFP* cells were grown and visualized as in B. Arrow: Ags1-GFP localization in the septum-like structure after mitosis and CAR assembly in the SIN mutant cell; arrowhead: septum-like structure detected by CW staining. Elapsed time is shown in minutes. Bar, 5 µm.

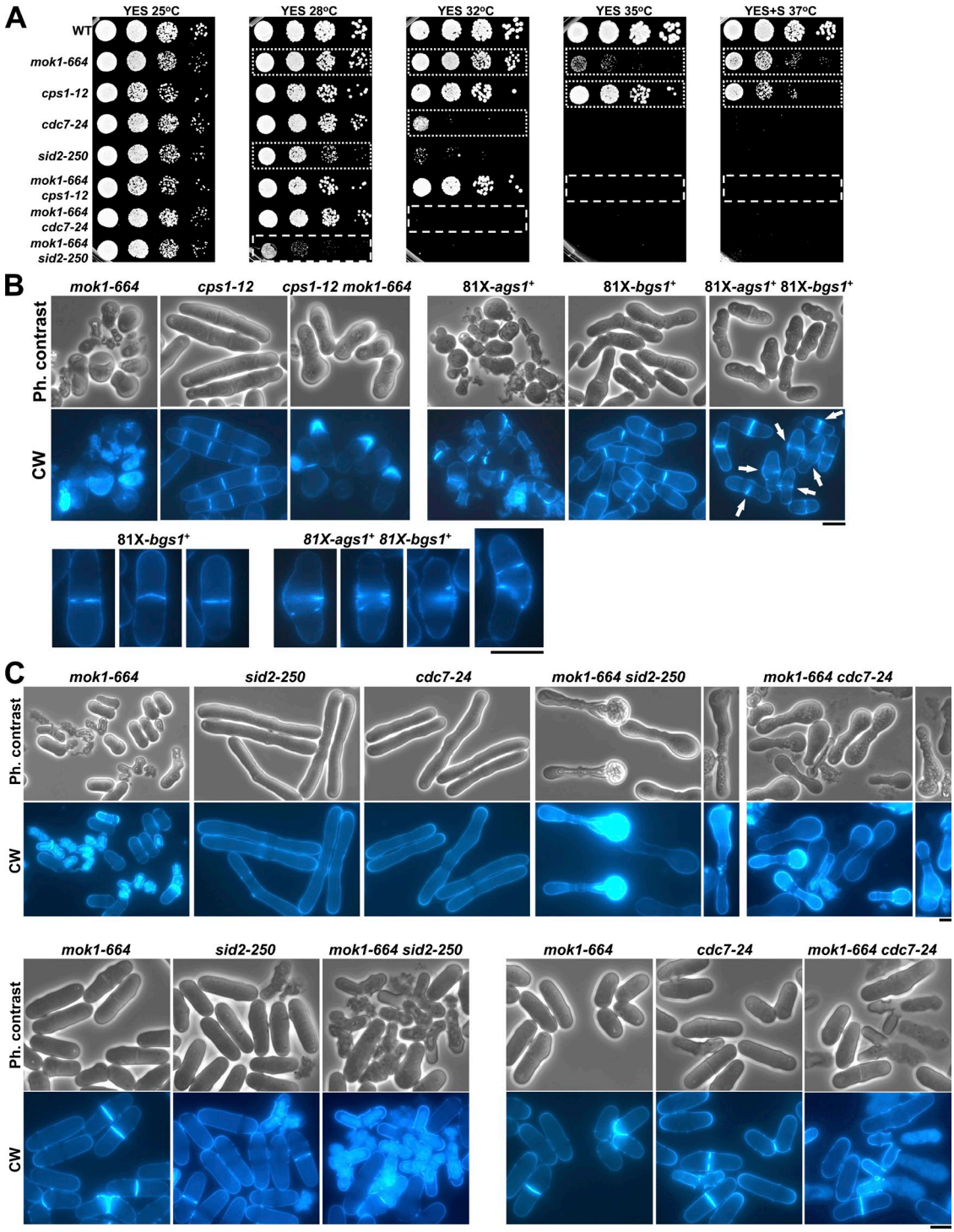

Figure S3. ***ags1⁺* presents genetic interactions with *bgs1⁺* and SIN genes.** The loss of Bgs1 function suppresses the lytic phenotype of Ags1 absence or *mok1-664* mutation and promotes strong cytokinesis defects. The absence of septa of the SIN mutants suppresses the septum lysis phenotype of *mok1-664* but promotes a new lysis at the poles. (A) The double mutants of *mok1-664* with the Bgs1 mutant *cps1-12* or with the SIN mutants *cdc7-24* or *sid2-250* are more thermosensitive than the single mutants. Early log-phase cells were adjusted to 10^7 cells/ml, 1:10 serial diluted, spotted onto YES and YES+S plates, and incubated at 25, 28, 32, 35, and 37°C for 3–4 d. The plates that displayed differences in growth between single and double mutant are shown. (B) The Bgs1 absence or *cps1-12* mutation suppresses the lytic phenotype of Ags1 absence or *mok1-664* mutation. In both cases the double mutants present strong septation defects. The *cps1-12 mok1-664* double mutation originates arrested cells with no septa and the combined Bgs1 Ags1 absence promotes stronger septation defects. The single and double *cps1-12* and *mok1-664* mutants were grown in YES+S at 37°C for 15 h. The single and double *ags1⁺* and *bgs1⁺* repression cells were grown in EMM+S+T for 15 h. The cells were visualized by phase-contrast and CW-staining microscopy. Arrow: increased septation defects of double *ags1⁺ bgs1⁺* repression cells. (C) The absence of septa of SIN mutants (high restrictive temperature) suppresses the septum lysis phenotype of *mok1-664* mutant but promotes a new lysis at the poles, whereas when the SIN mutants are able to form septa (low restrictive temperature) the septum lysis phenotype of *mok1-664* mutant is greatly increased. The single and double *cdc7-24* or *sid2-250* and *mok1-664* mutants were grown in YES for 6 h at 37°C (top panels) or for 2 h at 28°C (*sid2-250*) or 32°C (*cdc7-24*) (bottom panels). Cells were imaged as in B. Bar, 5 µm.

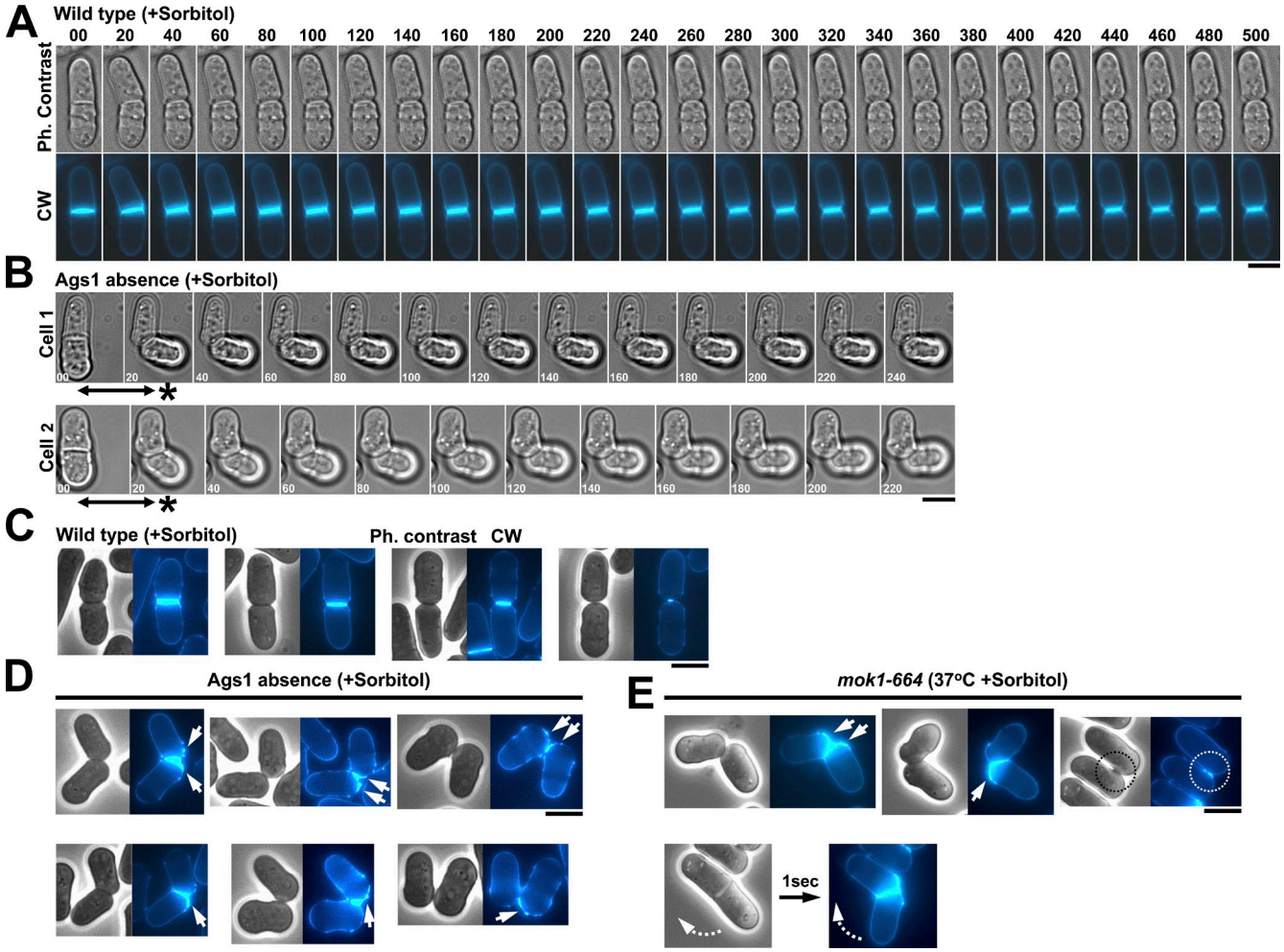

Figure S4. **Ags1-depleted or defective sister cells display a side-explosive cell separation due to tearing of a weak primary septum that remains attached to the new pole of one or both sister cells.** After the side-explosive cell separation the cells remain attached through the septum edging area. (A) Steady cell separation in wild-type cells. Cells were grown in EMM+S+T for 7 h and visualized by time-lapse phase-contrast and CW (5 µg/ml)-staining microscopy. Elapsed time is shown in seconds. (B) The absence of Ags1 originates cells with an immediate side-explosive cell separation. Cells were grown and imaged by time-lapse phase-contrast microscopy as in A. Asterisk: time needed after cell separation start for maximal new end curvature. (C) Wild-type cells separate symmetrically and gradually. Phase-contrast and CW-staining micrographs of log-phase wild-type cells grown in EMM+S+T at 28°C. (D) Ags1-depleted sister cells show the remains of primary septum in the pole of either both (top panels) or only one cell after asymmetrical side-explosive cell separation and tearing of primary septum. Ags1-depleted cells were grown in EMM+S+T for 8 h and visualized as in C. (E) The Ags1-defective *mok1-664* mutant shows the same side-explosive cell separation as the Ags1-depleted cells, with remnants of primary septum in one or both poles or just the septum edging. The cell separation occurs instantly (curved arrow) during the time spent for two image captures of the same cell. Cells were grown in YES+S at 37°C for 7 h and visualized as in C. Arrow: CW-stained remains of primary septum in the new end of both or just one sister cell. Circle: residual CW-stained primary septum in the septum edging. Bar, 5 µm.

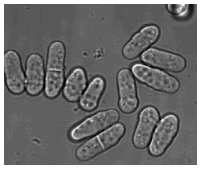

Video 1. **Representative field showing the lysis of either one or both sister cells at the beginning of cell separation of *S. pombe* Ags1-depleted cells.** 81X-*ags1*$^+$ cells were grown in the presence of thiamine for 3 h and imaged by time-lapse phase-contrast microscopy, using an inverted microscope (model IX71; Olympus) equipped with a Personal DeltaVision system (Applied Precision). Frames were taken every 20 s for 120 min. To decrease the movie size, the interval of frames around each cell lysis is exclusively shown.

Video 2. **Representative field showing the progressive and symmetrical cell separation of *S. pombe* wild-type cells.** Wild-type cells were grown in the presence of thiamine for 3 h and imaged by time-lapse phase-contrast microscopy, using an inverted microscope (model IX71; Olympus) equipped with a Personal DeltaVision system (Applied Precision). Frames were taken every 20 s for 89 min. To decrease the movie size, the frames exclusively show the cell separation stage.

Video 3. **Representative field showing the instantaneous and asymmetrical cell separation of *S. pombe* Ags1-depleted cells.** 81X-*ags1*$^+$ cells were grown in the presence of thiamine for 3 h and imaged by time-lapse phase-contrast microscopy, using an inverted microscope (model IX71; Olympus) equipped with a Personal DeltaVision system (Applied Precision). Frames were taken every 20 s for 89 min. To decrease the movie size, the frames exclusively show the cell separation stage.

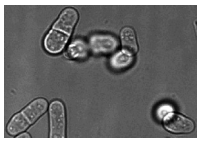

Video 4. **Representative field showing the instantaneous and asymmetrical cell separation of *S. pombe* Ags1-depleted cells growing in the presence of sorbitol.** 81X-*ags1*$^+$ cells were grown in the presence of thiamine and 1.2 M sorbitol for 4 h and imaged by time-lapse phase-contrast microscopy, using an inverted microscope (model IX71; Olympus) equipped with a Personal DeltaVision system (Applied Precision). Frames were taken every 20 s for 69 min. To decrease the movie size, the frames exclusively show the cell separation stage.

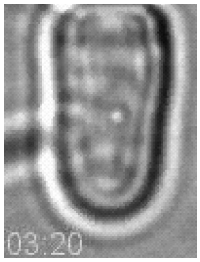

Video 5. **Progressive and symmetrical cell separation of a *S. pombe* wild-type cell.** Wild-type cells were grown in the presence of thiamine for 3 h and imaged by time-lapse phase-contrast microscopy, using an inverted microscope (model IX71; Olympus) equipped with a Personal DeltaVision system (Applied Precision). Frames were taken every 20 s for 6 min.

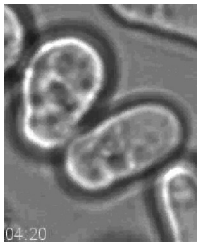

Video 6. **Instantaneous and asymmetrical cell separation of an Ags1-depleted cell.** 81X-*ags1*$^+$ cells were grown in the presence of thiamine for 3 h and imaged by time-lapse phase-contrast microscopy, using an inverted microscope (model IX71; Olympus) equipped with a Personal DeltaVision system (Applied Precision). Frames were taken every 20 s for 6 min.

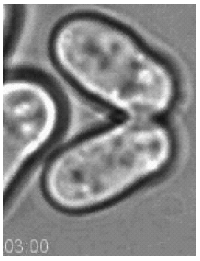

Video 7. **Instantaneous and asymmetrical cell separation of an Ags1-depleted cell.** 81X-*ags1*$^{+}$ cells were grown in the presence of thiamine for 3 h and imaged by time-lapse phase-contrast microscopy, using an inverted microscope (model IX71; Olympus) equipped with a Personal DeltaVision system (Applied Precision). Frames were taken every 20 s for 6 min.

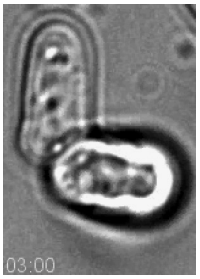

Video 8. **Instantaneous and asymmetrical cell separation of an Ags1-depleted cell growing in the presence of sorbitol.** 81X-*ags1*$^{+}$ cells were grown in the presence of thiamine and 1.2 M sorbitol for 4 h and imaged by time-lapse phase-contrast microscopy, using an inverted microscope (model IX71; Olympus) equipped with a Personal DeltaVision system (Applied Precision). Frames were taken every 20 s for 6 min.

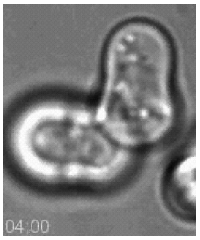

Video 9. **Instantaneous and asymmetrical cell separation of an Ags1-depleted cell growing in the presence of sorbitol.** 81X-*ags1*$^{+}$ cells were grown in the presence of thiamine and 1.2 M sorbitol for 4 h and imaged by time-lapse phase-contrast microscopy, using an inverted microscope (model IX71; Olympus) equipped with a Personal DeltaVision system (Applied Precision). Frames were taken every 20 s for 6 min.

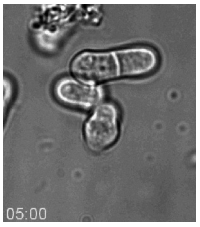

Video 10. **After instantaneous and asymmetrical cell separation, the Ags1-depleted sister cells remain attached by their lateral septum cell wall region for at least two cell cycles.** 81X-*ags1*$^{+}$ cells were grown in the presence of thiamine and 1.2 M sorbitol for 4 h and imaged by time-lapse phase-contrast microscopy, using an inverted microscope (model IX71; Olympus) equipped with a Personal DeltaVision system (Applied Precision). Frames were taken every 20 s for 20 min.

Table S1. **Fission yeast strains used in this study**

Strain	Genotype	Source
33	972 h^-	P. Munz[a]
256	*cps1-12 leu1-32 ura4-Δ18* h^-	J.C. Ribas
284	*leu1-32 ura4-Δ18 his3-Δ1* h^-	J.C. Ribas
285	*leu1-32 ura4-Δ18 his3-Δ1* h^+	J.C. Ribas
419	*leu1-32 ura4-Δ18* h^-	J.C. Ribas
420	*leu1-32 ura4-Δ18* h^+	J.C. Ribas
470	*leu1-32 ura4-Δ18 his3-Δ1* h^{90}	J.C. Ribas
317	*leu1-32/leu1-32 ura4-Δ18/ura4-Δ18 his3-Δ1/his3-Δ1 ade6-M210/ade6-M216* h^-/h^+	J.C. Ribas
439	*cdc3-6 leu1-32* h^+	J.C. Ribas
572	*cdc14-118 leu1-32 ade6-M210* h^+	J.C. Ribas
574	*cdc15-140 leu1-32* h^+	J.C. Ribas
577	*cdc15-140 leu1-32* h^-	J.C. Ribas
580	*cdc16-116 ura4-Δ18* h^+	J.C. Ribas
584	*tea2-1 leu1-32 ade6-M210* h^+	P. Nurse[b]
635	*mid1-366 leu1-32* h^+	P. Nurse[b]
899	*cdc11-119 leu1-32 his3-Δ1* h^+	J.C. Ribas
900	*cdc11-119 leu1-32 his3-Δ1* h^-	J.C. Ribas
953	*tea1-50 leu1-32 ura4-Δ18* h^+	J.C. Ribas
962	*leu1-32 ura4-Δ18 ade6 crn1⁺-GFP:KanMX6* h^+	F. Chang[c]
971	*leu1-32 ura4-Δ18 ade6 crn1⁺-GFP:KanMX6* h^-	F. Chang[c]
1723	*leu1-32 ura4-Δ18 his3-Δ1 bgs1Δ::ura4⁺* P_{bgs1+}*::GFP-bgs1⁺:leu1⁺* h^+	J.C. Ribas
1771	*sec8-1 leu1-32 ura4-Δ18* h^+	J.C. Ribas
1905	*leu1-32 ura4-Δ18 ade6 for3Δ::KanMX6* h^+	P. Perez[d]
2492	*leu1-32 ura4-Δ18 for3Δ::KanMX6* h^-	J.C. Ribas
2933	*leu1-32 ura4-Δ18 crn1⁺-GFP:KanMX6 for3Δ::KanMX6* h^+	J.C. Ribas
3137	*leu1-32 ura4-Δ18 ade6 myo52Δ::ura4⁺* h^+	M.H. Valdivieso[d]
2156	*mok1-664 leu1-32 ura4-Δ18* h^+	P. Pérez
4781	*mok1-664 leu1-32 ura4-Δ18* h^-	This study
2326	*sid2-250 leu1-32 ura4-Δ18 ade6-M216* h^+	J.C. Ribas
2327	*sid2-250 leu1-32 ura4-Δ18* h^-	J.C. Ribas
3065	*cdc7-24 ura4-Δ18* h^+	J.C. Ribas
2523	*cdc12-112 ura4-Δ18* h^+	P. Pérez
2525	*leu1-32 ura4-Δ18 leu1⁺::GFP-atb2⁺:ura4⁺* h^+	V. Simanis[e]
2086	*leu1-32 ura4-Δ18 his3-Δ1 ade6* $P_{nmt1\text{-}81X}$*-ags1⁺:ura4⁺* h^-	This paper
2100	*leu1-32 ura4-Δ18* $P_{nmt1\text{-}81X}$*-bgs1⁺:ura4⁺* h^-	J.C. Ribas
2234	*leu1-32 ura4-Δ18* $P_{nmt1\text{-}81X}$*-bgs1⁺* h^-	J.C. Ribas
1127	*leu1-32/leu1-32 ura4-Δ18/ura4-Δ18 his3-Δ1/ his3-Δ1 ade6-M210/ade6-M216 ags1⁺/ags1Δ::ura4⁺* h^-/h^+	This paper
1804	*leu1-32 ura4-Δ18 his3-Δ1 ade6-M210 ags1Δ::ura4⁺* h^- p41XH-*ags1⁺*	This paper
2881	*leu1-32 ura4-Δ18 his3-Δ1 ade6-M210 ags1Δ* h^- p41XH-*ags1⁺*	This paper
2939	*leu1-32 ura4-Δ18 his3-Δ1 ade6-M210 ags1Δ* 3′UTR_{ags1+}*::ags1*$_{3704\text{-}7233}$*:ura4⁺* h^- p41XH-*ags1⁺*	This paper
3166	*leu1-32 ura4-Δ18 his3-Δ1 ade6-M210 ags1Δ* 3′UTR_{ags1+}*::ags1⁺-GFP:leu1⁺:ura4⁺* h^-	This paper
3265	*ura4-Δ18 rlc1⁺-GFP:KanMX6* h^+	V. Simanis[e]
4004	*leu1-32 ura4-Δ18 his3-Δ1 ade6-M210 ags1Δ* 3′UTR_{ags1+}*::ags1⁺-RFP:leu1⁺:ura4⁺* h^-	This paper
4047	*leu1-32 ura4-Δ18 his3-Δ1 ade6 hht1⁺-RFP:KanMX6* h^+	P. Pérez
4090	*leu1-32 ura4-Δ18 his3-Δ1 bgs1Δ::ura4⁺* P_{bgs1+}*::3XHA-bgs1⁺:leu1⁺* h^+	J.C. Ribas
4223	*leu1-32? ura4-Δ18 ade6 ags1Δ* 3′UTR_{ags1+}*::ags1⁺-RFP:leu1⁺:ura4⁺ rlc1⁺-GFP:KanMX6* h^+	This paper
4083	*leu1-32 ura4-Δ18 his3-Δ1 ade6 ags1Δ* 3′UTR_{ags1+}*::ags1⁺-GFP:leu1⁺:ura4⁺ hht1⁺-RFP:KanMX6* h^+	This paper
3846	*mid1-366 leu1-32 ura4? his3-Δ1 ade6-M210 ags1Δ* 3′UTR_{ags1+}*::ags1⁺-GFP:leu1⁺:ura4⁺* h^+	This paper
3849	*cdc3-6 leu1-32 ura4? ags1Δ* 3′UTR_{ags1+}*::ags1⁺-GFP:leu1⁺:ura4⁺* h^+	This paper
3850	*cdc15-140 leu1-32 ura4? his3-Δ1 ade6-M210 ags1Δ* 3′UTR_{ags1+}*::ags1⁺-GFP:leu1⁺:ura4⁺* h^+	This paper
3852	*cdc11-119 leu1-32 ura4? his3-Δ1 ade6-M210 ags1Δ* 3′UTR_{ags1+}*::ags1⁺-GFP:leu1⁺:ura4⁺* h^-	This paper
3853	*cdc11-119 leu1-32 ura4? his3-Δ1 ade6-M210 ags1Δ* 3′UTR_{ags1+}*::ags1⁺-GFP:leu1⁺:ura4⁺* h^+	This paper
3855	*cdc14-118 leu1-32 ura4? ade6-M210 ags1Δ* 3′UTR_{ags1+}*::ags1⁺-GFP:leu1⁺:ura4⁺* h^-	This paper
3856	*cdc16-116 leu1? ura4-Δ18 his3-Δ1 ade6-M210 ags1Δ* 3′UTR_{ags1+}*::ags1⁺-GFP:leu1⁺:ura4⁺* h^+	This paper
3858	*tea1-50 leu1-32 ura4-Δ18 ade6-M210 ags1Δ* 3′UTR_{ags1+}*::ags1⁺-GFP:leu1⁺:ura4⁺* h^+	This paper
3861	*tea2-1 leu1-32 ura4? his3-Δ1 ade6-M210 ags1Δ* 3′UTR_{ags1+}*::ags1⁺-GFP:leu1⁺:ura4⁺* h^-	This paper
4014	*sid2-250 leu1-32 ura4-Δ18 ade6 ags1Δ* 3′UTR_{ags1+}*::ags1⁺-GFP:leu1⁺:ura4⁺* h^+	This paper

Table S1. **Fission yeast strains used in this study** *(Continued)*

Strain	Genotype	Source
4179	*sid2-250 leu1-32 ura4-Δ18 ade6 ags1Δ* 3′UTR$_{ags1+}$*::ags1⁺-GFP:leu1⁺:ura4⁺ hht1⁺-mRFP:KanMX6* h⁺	This paper
4016	*cdc12-112 leu1? ura4-Δ18 his3-Δ1 ade6-M210 ags1Δ* 3′UTR$_{ags1+}$*::ags1⁺-GFP: leu1⁺:ura4⁺* h⁺	This paper
4048	*leu1-32 ura4-Δ18 his3-Δ1 ade6-M210 ags1Δ* 3′UTR$_{ags1+}$*::ags1⁺-RFP:leu1⁺:ura4⁺ bgs1Δ::ura4⁺* P$_{bgs1+}$*::GFP-bgs1⁺:leu1⁺* h⁺	This paper
4067	*leu1-32 ura4-Δ18 his3-Δ1 ade6 ags1Δ* 3′UTR$_{ags1+}$*::ags1⁺-RFP:leu1⁺:ura4⁺crn1⁺-GFP:KanMX6* h⁻	This paper
4241	*cdc3-6 leu1-32 ura4-Δ18? his3-Δ1 ade6 ags1Δ* 3′UTR$_{ags1+}$*::ags1⁺-RFP:leu1⁺:ura4⁺crn1⁺-GFP:KanMX6* h⁻	This paper
4243	*leu1-32 ura4-Δ18 his3-Δ1 ade6 for3Δ::KanMX6 ags1Δ* 3′UTR$_{ags1+}$*::ags1⁺-RFP:leu1⁺:ura4⁺crn1⁺-GFP: KanMX6* h⁻	This paper
4245	*sec8-1 leu1-32 ura4-Δ18 ade6 ags1Δ* 3′UTR$_{ags1+}$*::ags1⁺-RFP:leu1⁺:ura4⁺crn1⁺-GFP:KanMX6* h⁻	This paper
4247	*leu1-32 ura4-Δ18 ade6 myo52Δ::ura4⁺ ags1Δ* 3′UTR$_{ags1+}$*::ags1⁺-RFP:leu1⁺:ura4⁺crn1⁺-GFP:KanMX6* h⁻	This paper
3954	*leu1-32 ura4-Δ18 his3-Δ1 ade6-M210 ags1Δ* 3′UTR$_{ags1+}$*::ags1⁺-GFP:leu1⁺:ura4⁺* h^{90}	This paper
4778	*cps1-12 mok1-664 leu1-32 ura4-Δ18* h⁻	This paper
4786	*leu1-32 ura4-Δ18 ade6 ags1Δ* 3′UTR$_{ags1+}$*::ags1⁺-GFP:leu1⁺:ura4⁺ bgs1Δ::ura4⁺* P$_{bgs1+}$*::3XHA-bgs1⁺:leu1⁺* h⁺	This paper
4790	*leu1-32 ura4-Δ18 his3-Δ1 ade6 ags1Δ* 3′UTR$_{ags1+}$*::ags1⁺-RFP:leu1⁺:ura4⁺ leu1⁺::GFP-atb2⁺:ura4⁺* h⁺	This paper
4800	*cdc15-140 leu1-32? ura4-Δ18 ags1Δ* 3′UTR$_{ags1+}$*::ags1⁺-RFP:leu1⁺:ura4⁺ rlc1⁺-GFP:KanMX6* h⁺	This paper
4802	*cdc11-119 leu1-32 ura4-Δ18 ade6 ags1Δ* 3′UTR$_{ags1+}$*::ags1⁺-RFP:leu1⁺:ura4⁺ rlc1⁺-GFP:KanMX6* h⁻	This paper
4825	*leu1-32 ura4-Δ18 ade6* P$_{nmt1\text{-}81X}$*-ags1⁺:ura4⁺* P$_{nmt1\text{-}81X}$*-bgs1⁺* h⁻	This paper
4844	*cdc7-24 mok1-664 leu1-32 ura4-Δ18* h⁻	This paper
4846	*sid2-250 mok1-664 leu1-32 ura4-Δ18* h⁺	This paper

[a]Institute of General Microbiology, University of Bern, Bern, Switzerland.
[b]Laboratory of Yeast Genetics and Cell Biology, The Rockefeller University, New York, NY.
[c]Department of Microbiology, Columbia University, New York, NY.
[d]Instituto de Biología Funcional y Genómica, Salamanca, Spain.
[e]School of Life Sciences, École Polytechnique Fédérale de Lausanne (EPFL), Lausanne, Switzerland.